NUREG/CR-0930, PT. II
UCRL/52638, PT. II

PUNCTURE OF SHIELDED RADIOACTIVE MATERIAL SHIPPING CONTAINERS, PART II--STATIC AND DYNAMIC TESTS OF LAMINATED PLATES

R. A. Larder
D. F. Arthur

Prepared for
U. S. Nuclear Regulatory Commission
by
Lawrence Livermore Laboratory

NOTICE

The views expressed in this report are not necessarily those of the U. S. Nuclear Regulatory Commission.

Available from U. S. Nuclear Regulatory Commission Washington, D. C. 20555

Available from National Technical Information Service Springfield, Virginia 22161

NUREG/CR-0930, PT. II
UCRL/52638, PT. II

PUNCTURE OF SHIELDED RADIOACTIVE MATERIAL SHIPPING CONTAINERS, PART II--STATIC AND DYNAMIC TESTS OF LAMINATED PLATES

R. A. Larder
D. F. Arthur

Manuscript Submitted: December 7, 1978
Date Published:

Prepared for
Research Division
U.S. Nuclear Regulatory Commission
Washington, D. C. 20555
Under Interagency Agreement DOE 40-550-75
NRC FIN No. A0127-8
by
Lawrence Livermore Laboratory
Livermore, CA 94550
operated by University of California
for the U.S. Department of Energy

FOREWORD

This document is the final report to the United States Nuclear Regulatory Commission (NRC) on the contract entitled, "Experimental and Analytical Assessment of Shipping Container Puncture Environments." The NRC project identification numbers are B&R 60193002, FIN A127-8. Personnel of the NRC Office of Nuclear Regulatory Research, Division of Safeguards, Fuel Cycle and Environmental Research requested this work.

CONTENTS

LIST OF ILLUSTRATIONS

LIST OF TABLES

ABSTRACT

We report on the development of improved analytical methods for predicting puncture of radioactive material shipping containers. We conducted 59 static and dynamic puncture tests of lead-backed, uranium-backed, and unbacked flat, circular, stainless steel plates with several mild-steel punch configurations. We found that analytical puncture prediction requires two essential elements: (1) a code that will accurately track stress and displacement throughout the event and (2) a criterion for identifying when and if puncture occurs. (The puncture event is not self-evident from the calculation.) We coupled the NIKE2D finite element code with the puncture criteria--a shear stress criterion for the lead-backed plates and a maximum effective plastic strain criterion for the uranium-backed plates; the results agreed very well with the test data.

INTRODUCTION

The puncture resistance of lead- and uranium-backed type AISI 316 stainless steel (SS) plates was established experimentally. Fifty-nine 12-in.-diam plates were statically and dynamically tested with cylindrical mild steel punches over a wide range of parameters. Extensive instrumentation and data reduction provided significant new information about the phenomena of puncture of laminated plates. Our tests provide insight and data that can be applied empirically to cask puncture problems. The circular plates can be considered subscale end plates of typical shipping containers. The data also provide a basis for validating finite element codes intended for puncture calculations. This part of the final project report describes the tests and the results. All the dynamic test data are recorded on microfiche and attached to this report.

SUMMARY OF PUNCTURE TESTS

The parameters that were varied in this investigation were punch diameter, test plate thickness, backing material, and test temperature. Usually, the backing thickness was equal to the punch diameter for lead-backed plates. Only limited variation in backing thickness and punch edge radius was accomplished during the static tests. Impact velocity was varied in the dynamic tests by changing the drop height but, where possible, the drop height was kept at the regulatory 40 in. The test plate diameter, material, and punch material remained the same throughout the tests. Table 1 summarizes the static and dynamic test conditions and results, lists the test numbers referenced on michrofiche, and gives the average penetration force and energy for the plates that failed for each test configuration.

TEST SPECIMEN AND FIXTURE DESCRIPTION

Figure 1 shows a typical test configuration of three 12-in.-diam plates clamped together at their circumference in the test fixture. The SS test plate is backed by either a lead or uranium plate followed by another

TABLE 1. Plate puncture tests.

Punch diam-in.	0.6	0.6	0.6	0.6	0.6	0.6	0.6	0.6	0.6	0.936	1.5	1.5	1.5	1.5	1.5	1.5	1.5	1.5	0.6	0.6	0.936	1.5
Nominal plate thick.	0.05	0.1	0.1	0.1	0.1	0.2	0.2	0.2	0.375	0.312	0.125	0.125	0.125	0.25	0.25	0.25	0.5	0.5	0.05	0.05	0.312	0.125
Actual plate thick.	0.05	0.118	0.104	0.119	0.119	0.2	0.2	0.2	0.415	0.323	0.117	0.117	0.117	0.262	0.262	0.262	0.54	0.54	0.05	0.05	0.323	0.117
Backing material	Pb	None	Pb	Pb	Pb	Pb	Pb	Pb	Pb	Pb	Pb	Pb	None	Pb	Pb	Pb	Pb	Pb	U	U	U	U
Backing thick-in.	0.6	0.0	0.6	0.936	1.5	0.6	0.6	0.6	0.6	0.936	1.5	1.5	0.0	1.5	1.5	1.5	1.5	1.5	0.4	0.4	0.624	1.0
Test temp ^{o}F	75.	75.	75.	75.	75.	75.	200	400	75.	75.	75.	75.	75.	75.	200	400	75.	75.	75.	75.	75.	75.
Static																						
Punch edge radius	0	0	0	0	0	0	0	0	0	0	0	1/16	0	0	0	0	0	1/16	0	0	0	0
Test no.'s	1S	18S	7S	16S	17S	3S	10ST	11ST			6S	15S					5S	20S	2S	8S		12S
						14S			-	-			-	-	-	-	13S[a]		4S		-	
Av pen. force-kips	7.	12.5	13.8	15.5	16.7	25.4	21.5	16.0	-	-	39.0	40.0	-	-	-	-	175.	202.	32.5	29.5		200.
Av pen. energy-kip-in.	2.3	5.28	5.6	6.85	7.18	14.5	11.5	7.3	-	-	23.3	26.0	-	-	-	-	265.	307.	10.0	14.0	-	100.
Dynamic																						
Drop ht-in.	var.	-	10	-	-	var[c]	-	-	40	40	40	-	40	40	40	40	118	-	var.	40	var.	var.
Test no.'s	1D		22D			5D			16D[a]	23D	12D		39D[a]	26D	35D	36D	28D[a]		8D[a]	32D	15D	30D
	2D		25D[a]			6D			18D[a]	24D	13D		41D	34D[a]			29D		9D	33D[a]	17D[a]	31D
	3D[a]	-		-	-	19D	-	-	27D[a]	37D[a]	14D[a]	-						-	11D		38D	
	4D[a]					20D															40D[a]	
	7D[a]					21D[a]																
	10D																					
Av pen. force-kips	8.1	-	b	-	-	25.9	-	-	-	67.0	46.5	-	31.1	86.8	81.5	56.7	176.5	-	39.5	38.2	120.	217.
Av pen energy-kip-in.	2.34	-	5.7[b]	-	-	12.6	-	-	-	52.8	22.9	-	21.6	68.4	64.0	45.3	243.	-	10.2	31.0	174.	110.

[a]Plate did not fail.

[b]No data recorded. Average penetration energy based upon average impact energy of plate that failed and plate that did not fail.

[c]No difference in puncture force or energy when dropped with same energy and one-half velocity.

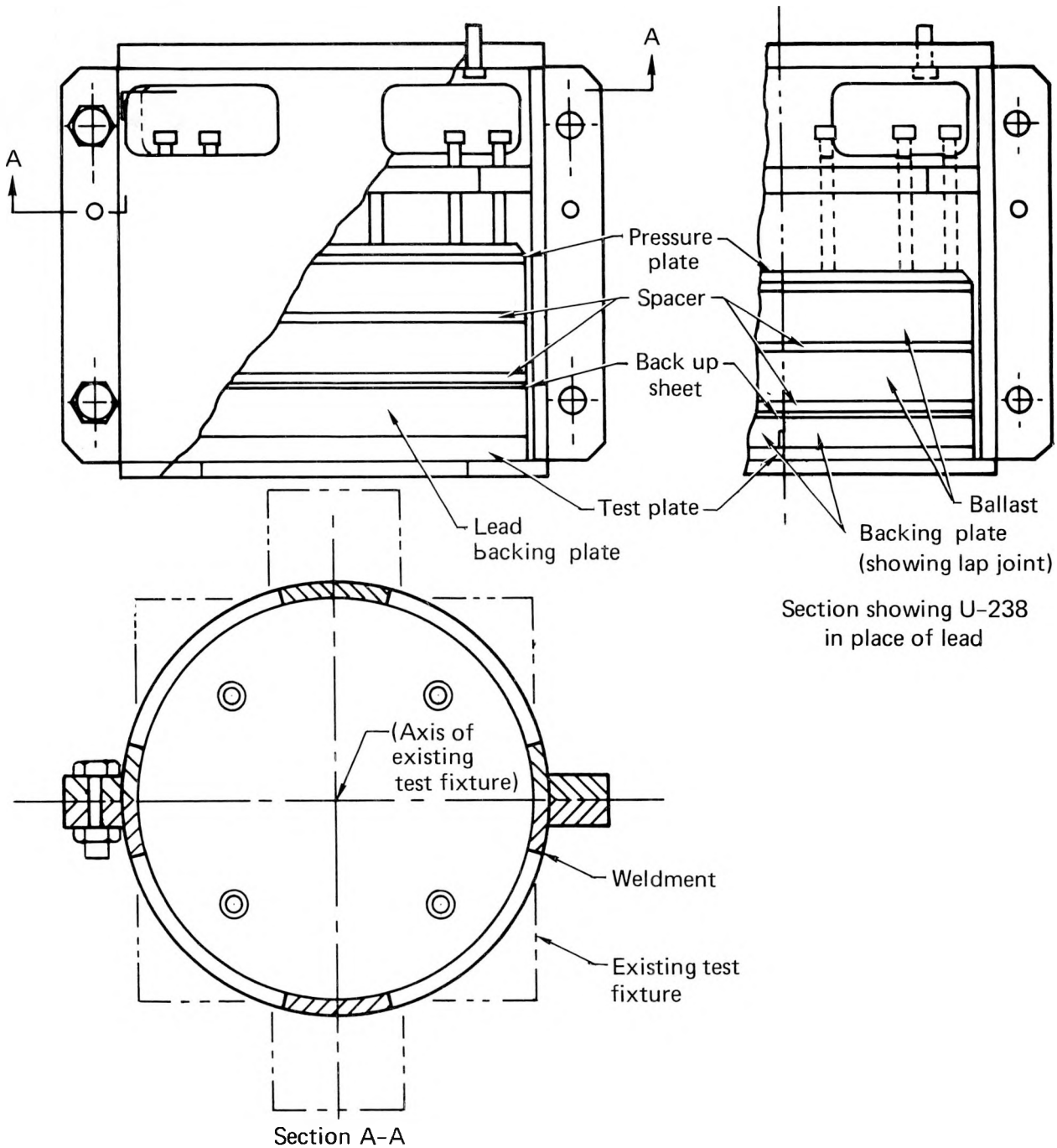

FIG. 1. Test fixture assembly.

SS plate 0.05 in.-thick simulating the internal structure of a shipping container. Three stainess steel plates were tested without backing. A number of annular steel spacers, 1/4-in. thick with an 8-in. i.d., are placed behind the 0.05-in. SS back plate. The test plates are clamped between the spacers and an 8-in.-i.d. annular plate welded to the end of the cylindrical portion of the test fixture.

The test fixture is a 12-in.-i.d. cylindrical steel tube with three annular plates welded to it: one at each end and one internally. The internal annulus is drilled and tapped for cap screws that clamp the spacers and test plates against the annular end plate. The assembly is bolted to the drop test fixture through holes in the top plate. Additional ballast plates of lead or uranium can be clamped behind the spacer plates for the dynamic tests.

The vertical separation plane in the fixture and the heavy longitudinal flanges welded outside the cylinder facilitate test fixture disassembly. Four large bolts clamp the two halves of the fixture together. The diameter of the fixture minimizes edge effects and accommodates existing test equipment. The size of the test fixture permits efficient handling with available mechanical hoists and minimizes manpower requirements. A test assembly can be disassembled and reassembled--exclusive of instrumentation--in less than 60 min by a crew of three men. The heaviest backing plate weighs 75 lb. Three fixtures permit simultaneous static and dynamic testing and one assembly can be built up while another is being tested.

Figure 2 shows the three punch geometries. To minimize cost and project complexity, we used subscale punches. These punches are between 1/10 and 1/4 the regulatory 6-in.-diam by 8-in. long dimensions. Because punch yielding was experienced, we used a new punch for each test. We machined the punches from Type A-36 steel bar stock with the length 4/3 of the diameter in all cases. The punch diameters are 0.06 in., 0.936 in., and 1.5 in. In these tests, the ratio of the punch diameter (d) to plate thickness (t) covers the range of 1.5 to 12.8. This is equivalent to shipping cask structural thicknesses of 1/2 in. to 4 in. for a 6-in.-diam punch. We attempted to maintain d/t ratios of 3, 6, and 12 for all three punches as well as a d/t

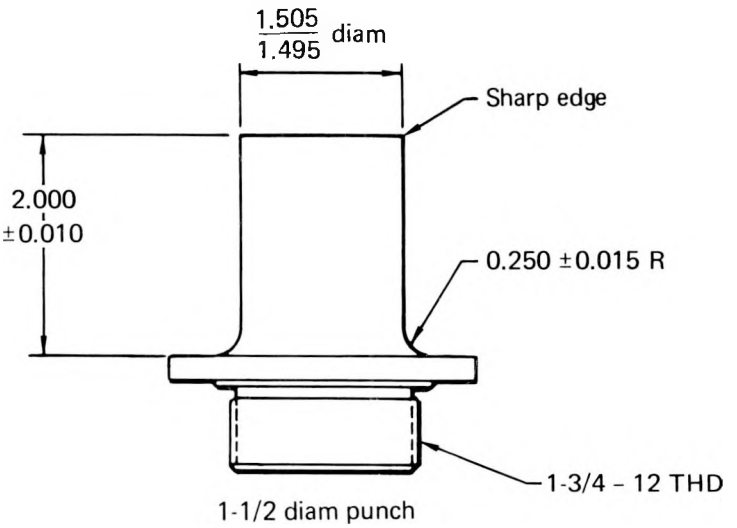

1-1/2 diam punch

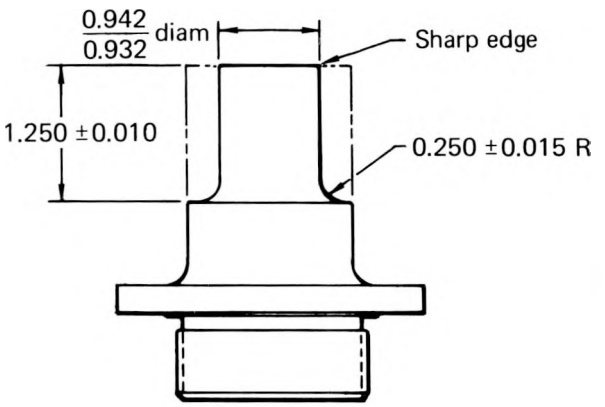

15/16 diam punch

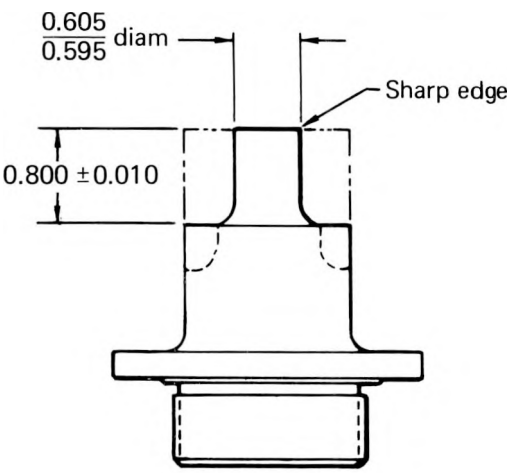

0.6 diam punch

FIG. 2. Punch geometries.

ratio of 1.6 for the smallest punch. We used standard plate thicknesses whenever possible to avoid machining the plate surfaces.

Of the 59 plates tested, 41 were lead-backed, 15 uranium-backed, and three unbacked. It is important to note that no data existed on the puncture resistance of uranium-backed plates prior to this project. This situation coupled with the high cost--over $900 each--of each uranium plate limited the number of tests of uranium-backed plates and thus introduces uncertainty in our results.

Cost was also the primary justification for maintaining a constant ratio between the punch diameter and the backing thickness. Systematic variation in all of the parameters important to plate puncture would have required a prohibitively large number of tests. In one series of static tests, we varied the backing from zero to 2.5 times the punch diameter, with all other parameters remaining constant. We conducted two dynamic tests on unbacked plates.

For uranium-backed plates, we used uranium of a thickness that provided the same amount of radiation shielding as that of lead. For example, a punch diameter of 1.5 in. requires 1.0 in. of uranium backing because this amount of uranium is the same as a 1.5-in. lead backing.

Because uranium-shielded casks are often fabricated of jointed uranium rings, we experimentally evaluated the effect of such a joint by fabricating several flat circular plates formed of two "D"-shaped semicircular plates with step joints machined into the diameters. These two semicircular plates were then placed into the test fixture behind a test plate, as shown in Fig. 1.

Strain gages monitored strains in the plate and punch during testing. Punch force and total deflection were recorded for each test. Accelerometers were epoxied on the surface of the test plate and mounted on the ballast for the dynamic tests. Figure 3 is a composite instrumentation diagram showing plate and punch instrumentation layouts for all of the tests except those with jointed-uranium backing. Figure 4 shows strain gage installation on the

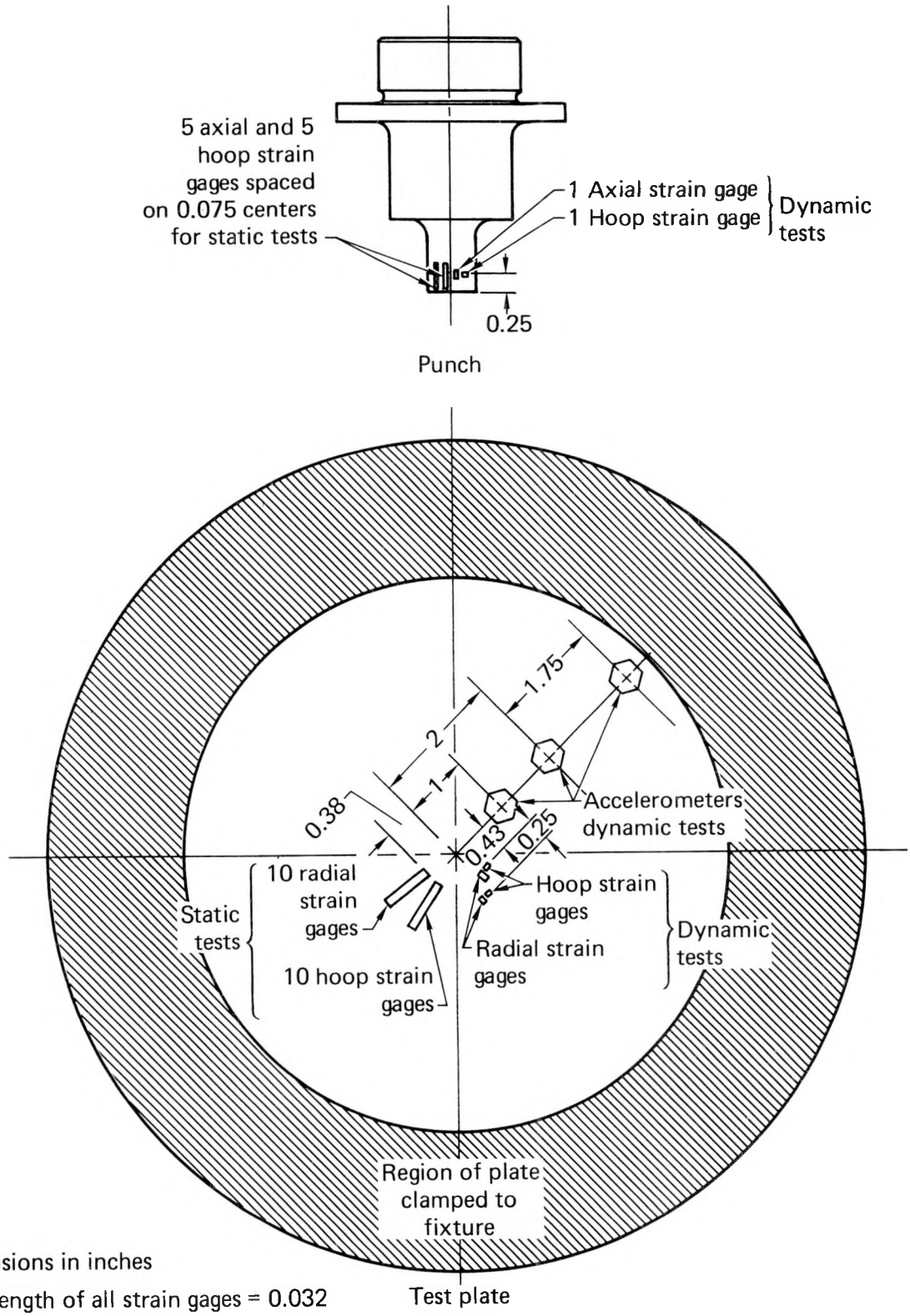

FIG. 3. Composite instrumentation drawing.

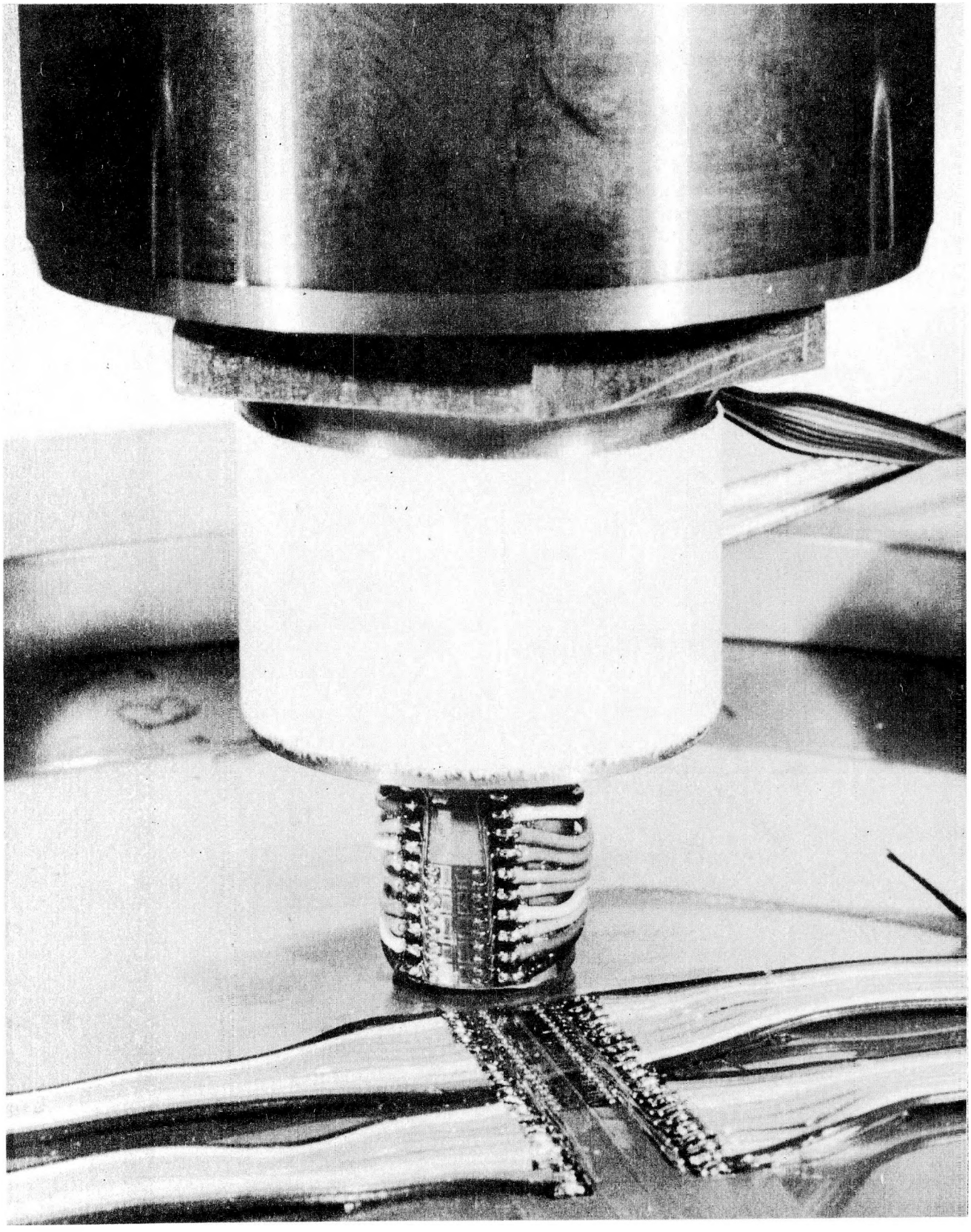

FIG. 4. Plate and punch strain gage installation.

plate and punch in a static puncture test. The jointed uranium was instrumented so as to monitor strains and accelerations along and perpendicular to the joint.

MATERIAL PROPERTIES COUPON TESTS

Coupons were cut from the outer two in. of several plates--the area of least deformation. Tensile coupons were cut from the SS and uranium plates, and compression coupons were taken from the lead plates. We used the stress-stain curves in the finite element analyses. (Samples of these curves and the average strength data are in Part I of this report.) No mild steel coupons were tested because adquate material property information was obtained from the punch strain gages, load cell, and posttest measurements of the deformed punch. Figure 5 shows the static and dynamic true stress-strain curve inferred from the puncture test data for the Type A-36 mild steel punches. The ultimate compression strength of the punch material was never reached in the puncture tests, although compressive strains in excess of 50% were recorded.

STATIC TEST PROCEDURE

In the static test, the assembled test fixture was held in the center of the lower platen of a 500,000-lb-capacity universal testing machine, as shown in Fig. 6. The punch was screwed into the center of the upper platen or moving part of the machine and then forced into the center of the test plate until penetration occurred. Typically, the load was applied in small increments and held constant until the punch deflection stabilized. Instrumentation readings were then recorded. At the higher loads, it often took several minutes for the deflection to stabilize. We attribute this delay, which occurred in all tests, to slippage in the test fixture.

To minimize the test duration for the elevated temperature tests, the load was continuously increased from zero to the penetration load in a few minutes. We periodically sampled the strain gage data as the load increased. To establish the sensitivity of the test results, we applied the procedure to a test configuration identical to one previously tested. Figure 7 shows plots of

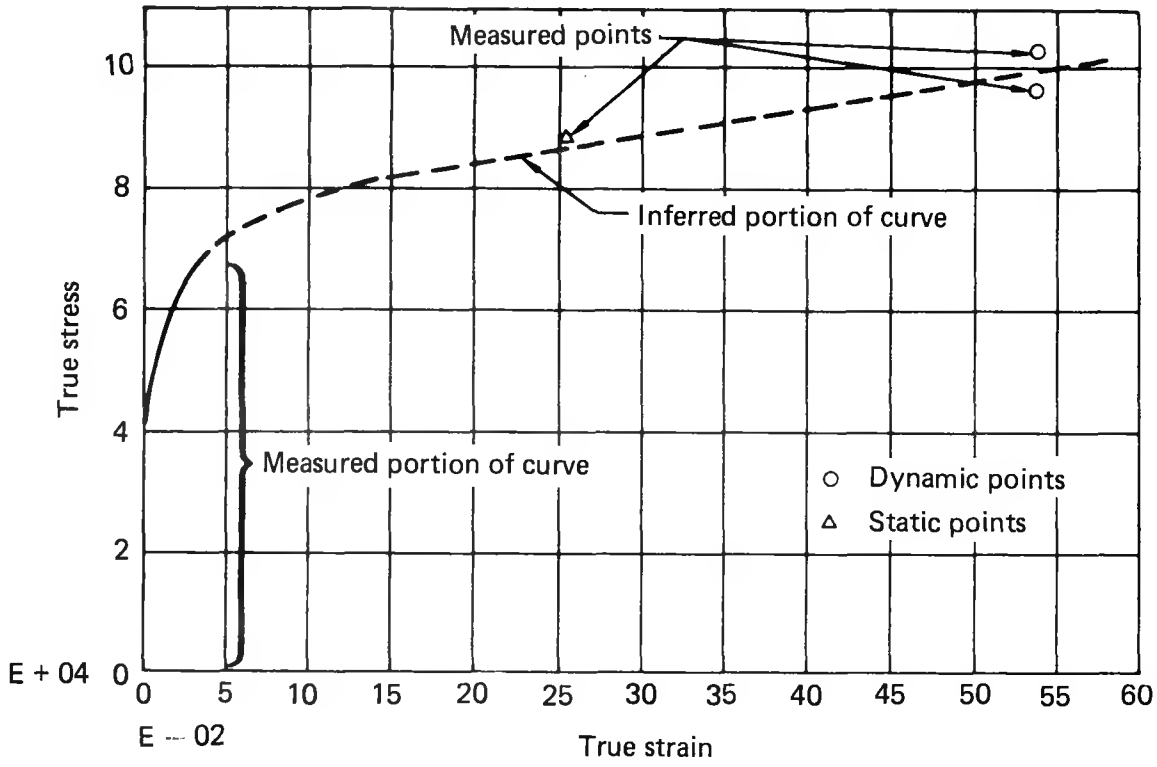

FIG. 5. Static and dynamic stress-strain curve for type A-36 steel.

force vs deflection for two 0.2-in. lead-backed plates tested at room temperature in both ways. The existence of slippage in the test fixture is confirmed by the minor differences in the load deflection curves that resulted when the test technique was varied.

For the elevated temperature tests, the fixture was mounted on the test machine and wrapped with electrical-resistance heater tapes and thermal insulation. As heat was added, the temperatures of the test and backing plates were monitored until the required test temperature was reached and the thermal gradients in the plates were minimized. Less than $3^{o}F$ temperature difference existed between the test and backing plates when the puncture test was begun. The punch was not heated during the test.

Although strain data were recorded up until plate failure, the strain gages did not always behave reliably to the moment of failure. Evidently, the large strains were beyond the capability of the gages or adhesive. The finite element calculations predict strains in excess of 50% in both the plate and the punch, but the strain gages were unable to measure any strains beyond

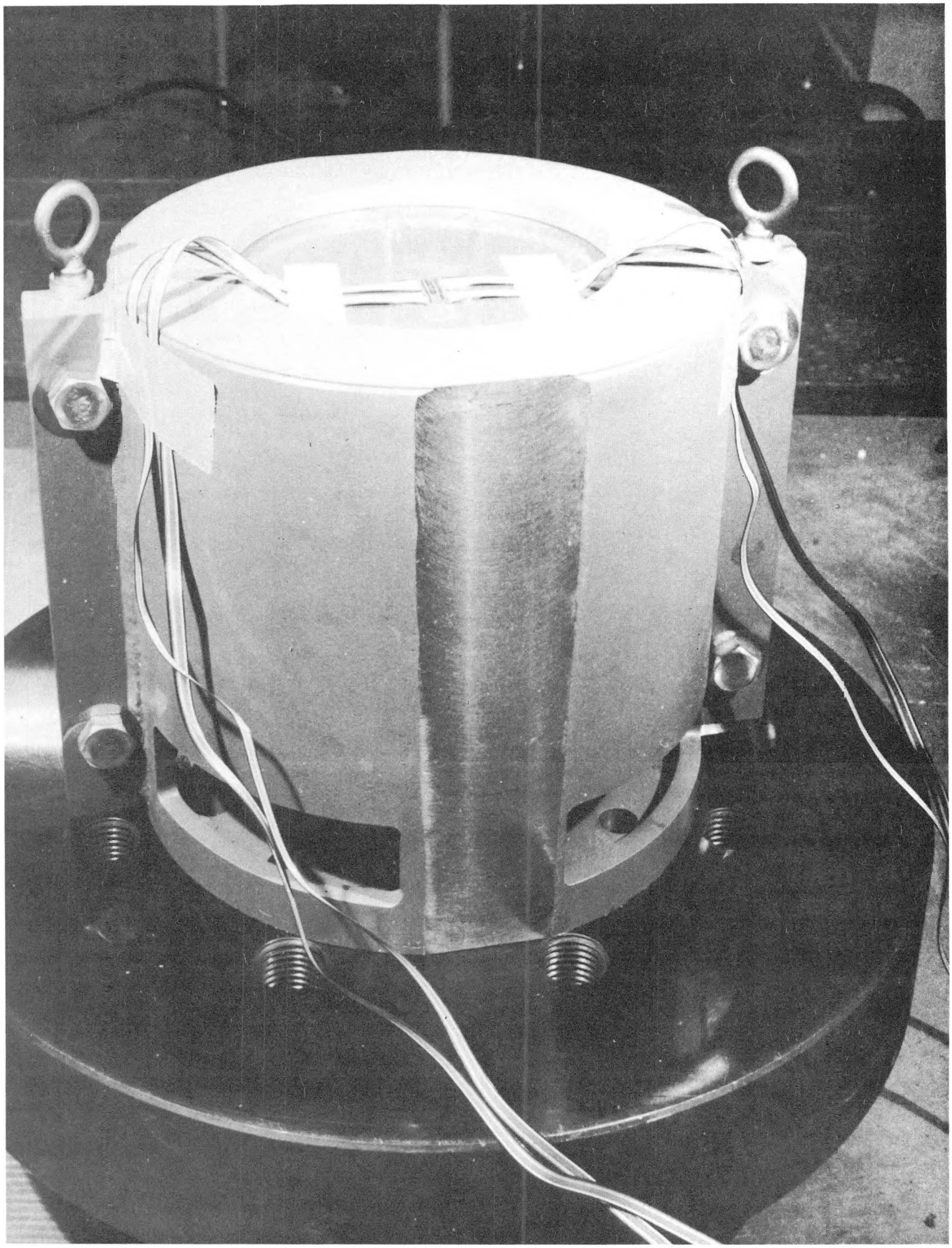

FIG. 6. Static test fixture.

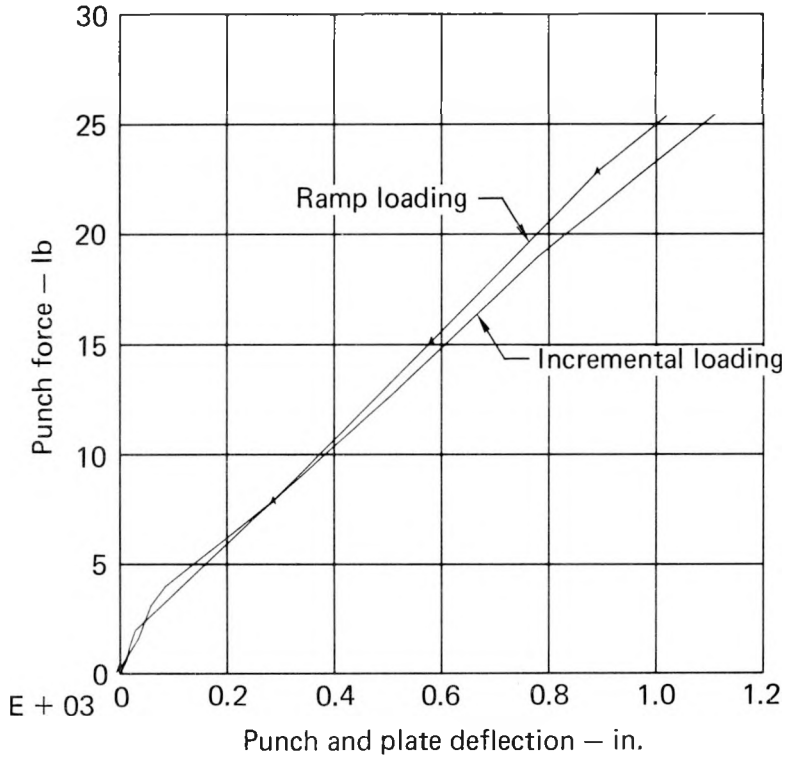

FIG. 7. Comparison of static test methods for 0.2-in. lead-backed SS plate.

about 4%. A strain of 4% would usually occur near one half of the penetration load. The punch force and deflection measurements were reliable up to the point of failure on all of the static tests.

DYNAMIC TEST PROCEDURE

In the dynamic tests, the test fixture bolts to the bottom of the drop carriage of an existing shock testing machine, as shown in Fig. 8. The drop carriage is hoisted to the desired height and held there by a quick-release mechanism. The carriage is guided by two 2-in.-diam chrome-plated steel rods on either side of the fixture. These guide rods ensure that the punch impacts the plate within 1/4 in. of the center. The guide rods also ensure parallel impact between the face of the punch and the surface of the plate within 1^{o}.

To measure the punch force, we screwed the punch directly into a load cell. The load cell is mounted on a 2600-lb solid steel reaction mass that is supported by an 8-in.-thick reinforced concrete floor that is founded on the earth. An accelerometer is mounted on the reaction mass. Two load cells of

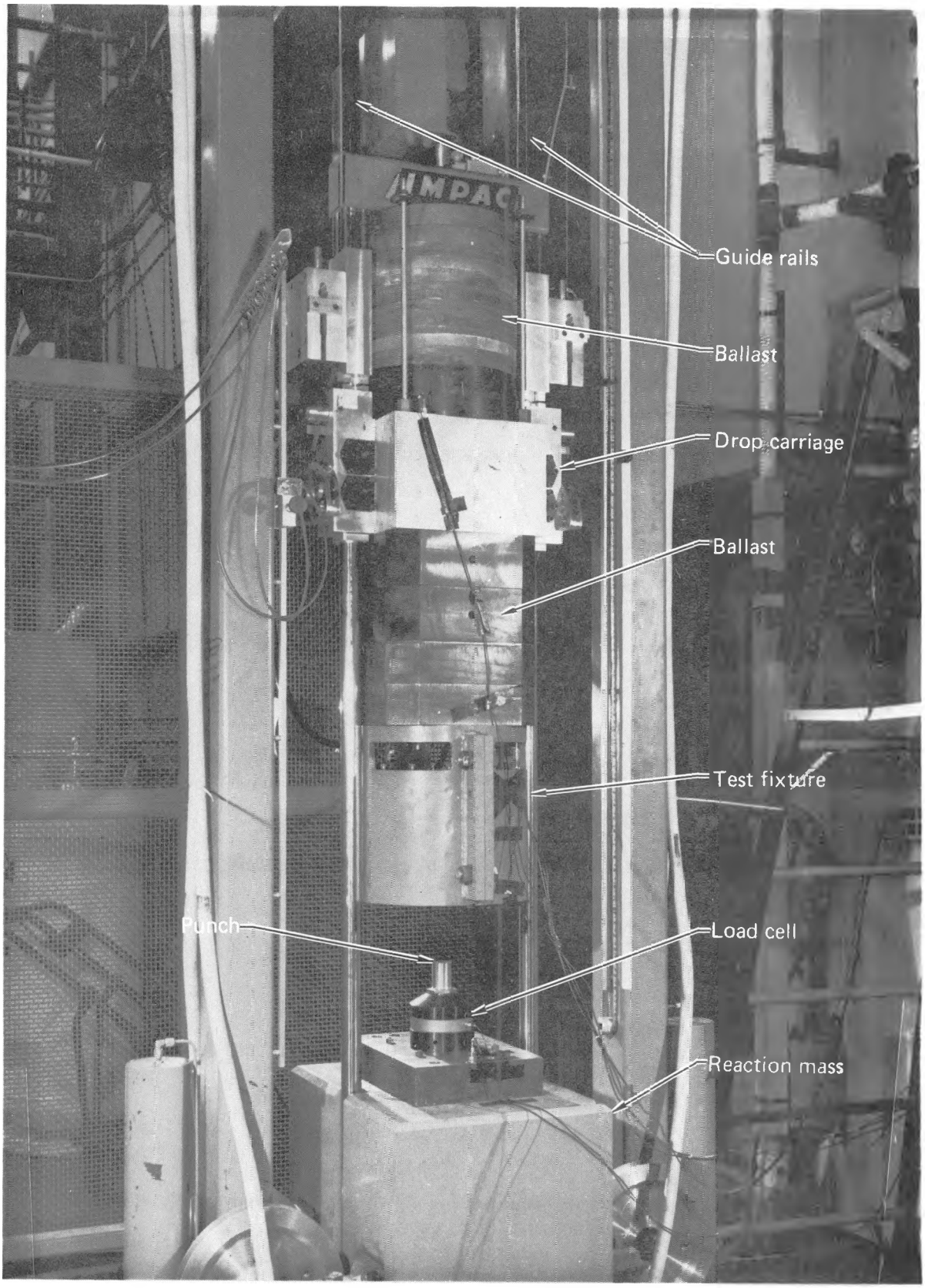

FIG. 8. Dynamic test setup.

different design were used in the tests. A 100,000-lb-capacity strain-gage-type load cell was used for the lower energy drops, and a 200,000-lb-capacity piezoelectric load cell was used for the higher energy drops. The load cells were chosen for their high stiffness and their ability to maintain maximum system rigidity. According to previous calibrations, neither load cell produced over 0.005-in.-deflection at 100% of load capcity.

Two break-leads are mounted 4 in. apart and above the impact point. Carriage transit time between the two break-leads measures the impact velocity. In general, the impact velocity was less than 5% below the velocity calculated for free fall from the measured drop height. Complete, valid time histories were recorded for the punch force and carriage accelerations for the 36 of the 41 dynamic tests. Three failures were due to faulty triggering and two were due to changeover to an unfamiliar F/M data system when the regular digital system was unavailable. The strain gages again produced useful data only up to about 4% strain before they became unreliable. The accelerometers mounted to the plate in Fig. 3 did not always remain glued to the surface during the impact event. The time history shows the exact time when the data cease to be valid with sharp discontinuities.

Because of practical limitations on control of the ballast mass, 19 of the 41 tests were not dropped at the regulatory 40-in. height. The minimum weight in this test setup was 360 lb. The incipient penetration energy of several plates was lower than the 14,400 in.-lb produced by dropping 360 lb 40 in. On the other hand, puncture of the 1/2-in. plate from 40 in. would have required a weight greater than 6000 lb. This was not practical, because the hoist that raises the drop carriage is limited to 4000 lb. By stacking lead and depleted uranium on top of the drop carriage and solid steel blocks between the test fixture and the carriage it was possible to produce a maximum weight of 1950 lb. The maximum height possible with our test setup was 118 in. which produced enough impact energy to just fail the 1/2-in. lead-backed plate.

The elevated temperature drop tests were conducted in the following manner. The cylindrical test fixture holding the plates was preconditioned for several hours in an oven. After stabilizing at slightly above the desired test

temperature, the fixture was removed from the oven, quickly bolted to the drop carriage, and dropped onto a room temperature punch. Thermocouples were used to monitor the temperature of the test plates during this process.

DATA REDUCTION

All test data were converted to digital format and stored on the LLL IBM Photostore for subsequent data reduction. The raw data were also replotted on 105-mm microfiche. The only data reduction performed on the static test data was integration of the punch force vs deflection curves to obtain the total puncture energy.

For the dynamic tests, the raw data consisted of punch force, strains, and accelerations as a function of time. By integrating the accelerations, the velocities and displacements as a function of time were obtained. Time was eliminated as a parameter of the data, and plots of displacement and strain as a function of punch force were obtained for comparison with the static data. Finally, integration of the force deflection curves showed the work or energy absorbed by the plate and punch. As a check on this work done on the system, we calculated the kinetic energy of the system as measured by the velocity squared times the mass. Figure 9 demonstrates how a typical test obeys the conservation of energy law. Since the kinetic energy is derived from the acceleration data alone and the work performed is based upon both the acceleration and load cell data, Fig. 9 also provides a convenient cross-check of the accuracy of the data.

LAMINATED PLATE TEST RESULTS

The data obtained from the 59 tests are attached to this report in the form of microfiche. Typical curves of the more interesting comparisons between various tests are presented and discussed along with examples of our reduction.

In the static tests, force vs deflection was obtained directly during every test. Figure 10 shows typical examples for three different plates.

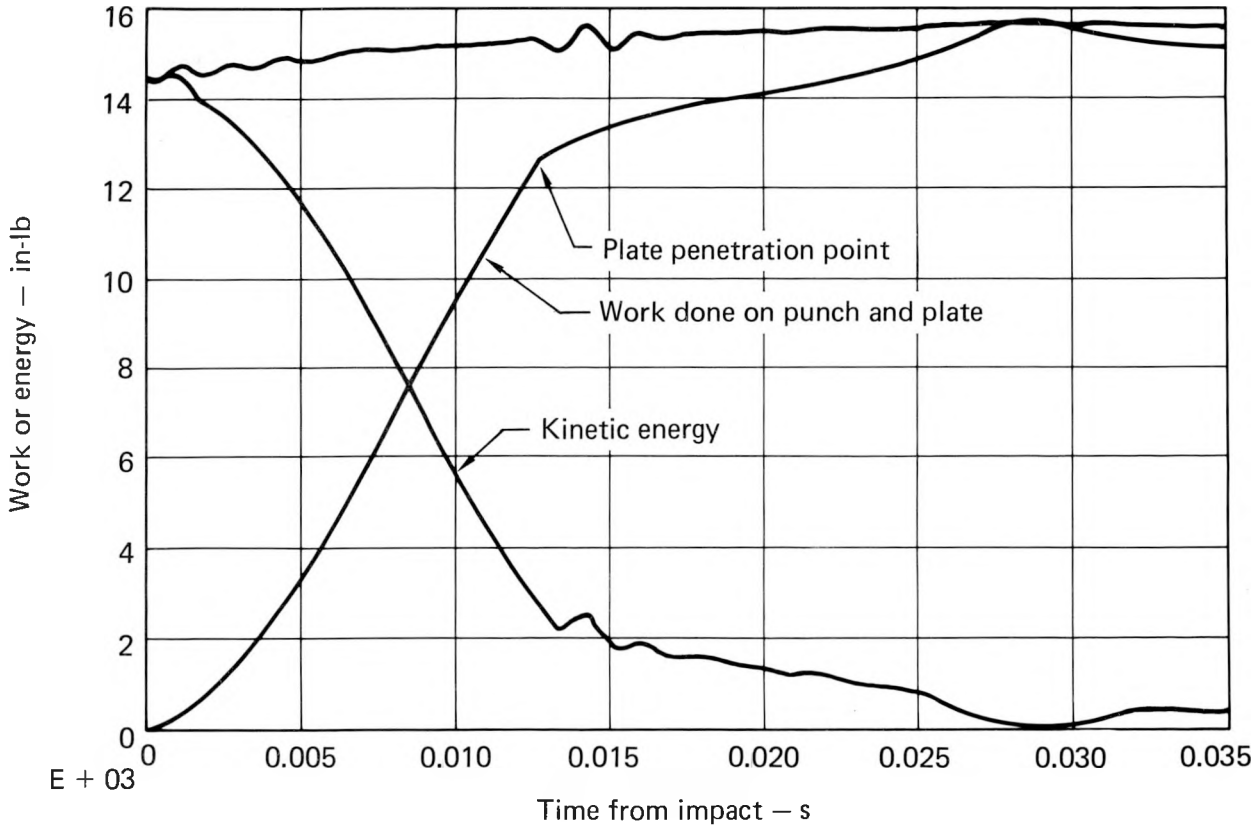

FIG. 9. Kinetic energy and work done during test 20D.

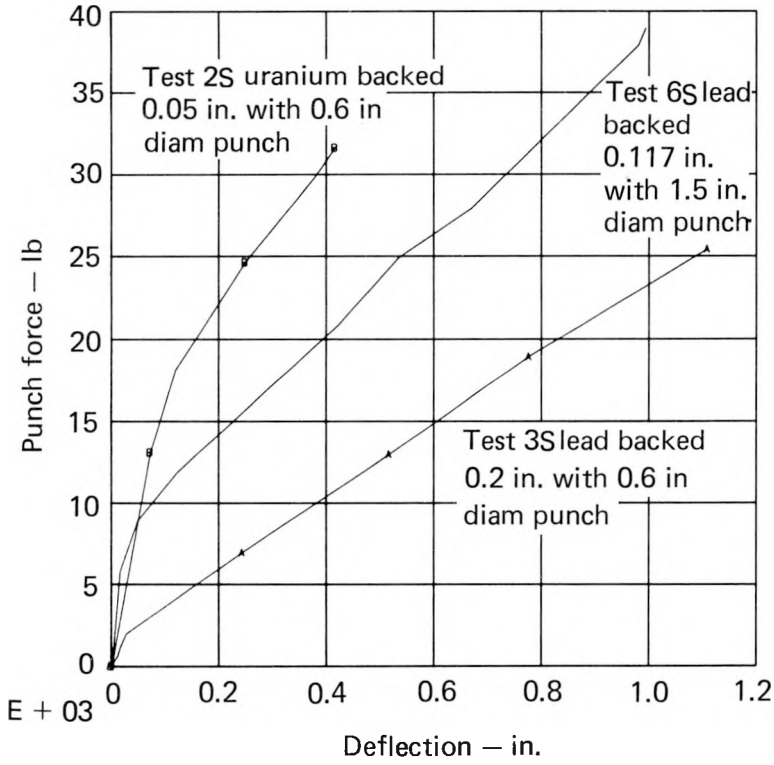

FIG. 10. Typical force vs deflection curves for static plate puncture tests.

Figure 11 shows typical plots of punch strain vs punch force for the same three tests of Fig. 10. The punch strain is measured about 0.35 in. down from the end of the punch in contact with the plates and parallel to the centerline of the punch. This measurement demonstrates that the punch yields significantly in some tests and not in others.

Bending of the plate produces compressive strain in the strain gages on the side of the test plate in contact with the punch. Figure 12 shows how tensile membrane strains dominate the plate deformations after the deflections become large in tests 2S, 3S, and 6S. This figure shows strains measured at approximately 0.13 in. from the punch edge.

In the dynamic tests, the data are recorded as a function of time. All backed plates produced force-time histories with very similar features: The general characteristics show that the force increased very rapidly to a plateau immediately after impact. Following a period of overshoot, higher mode oscillation damped in the first few milliseconds followed by a relatively gradual increase to the maximum load. After reaching the maximum load, the

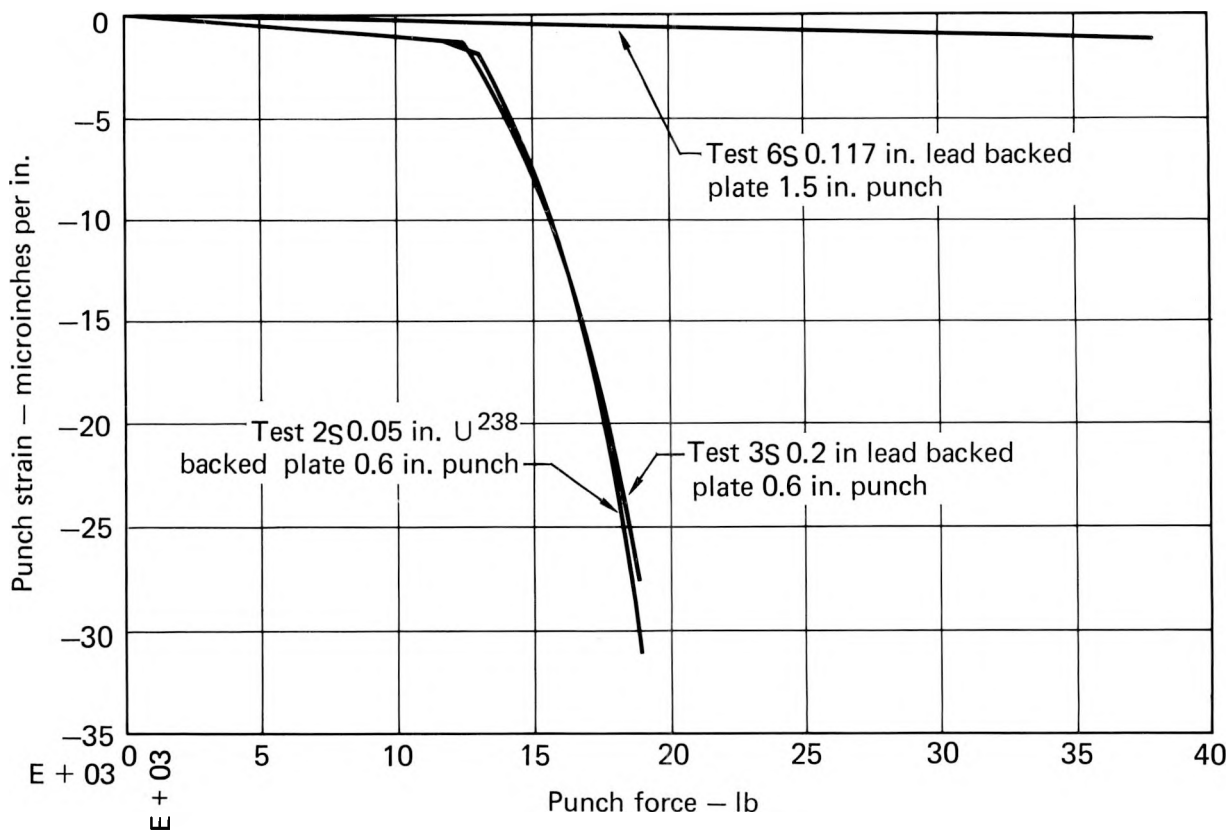

FIG. 11. Typical punch strains for static tests.

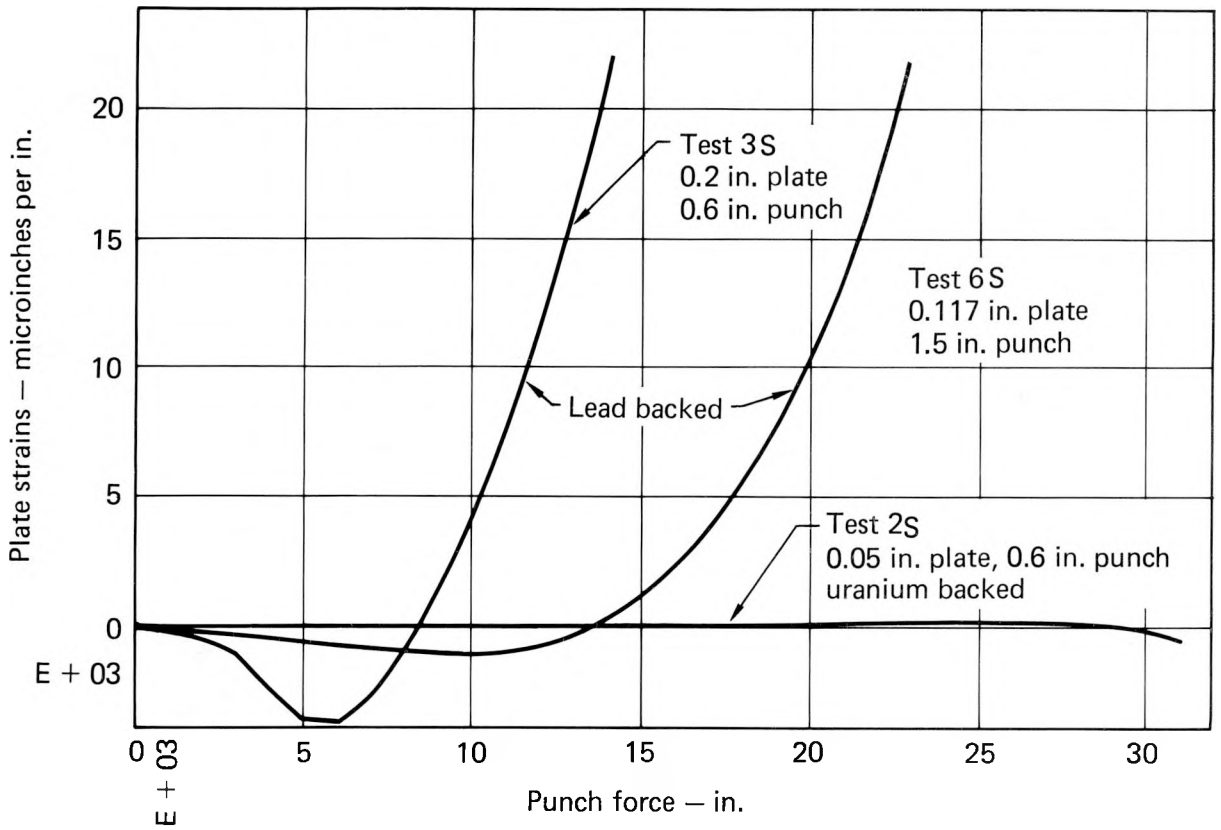

FIG. 12. Typical plate strains during static tests.

waveform takes on two easily distinguishable characteristics. If the plate does not fail, the load decreases to zero gradually as the plate rebounds, but faster than it increased. If the plate fails, the load decreases immediately, followed by a short period of oscillation. Figure 13 shows typical responses for two plates impacting the punch at energies above and below the incipient puncture energy. From these plots, it is easy to determine the exact instant of failure in all tests on lead-backed plates. For uranium-backed plates, higher vibration amplitude and frequency and a different mode of failure makes the instant of failure more difficult to discern.

Figure 14 demonstrates the importance of vibration in the ballast acceleration vs time plot for the punch penetration test in Fig. 13. On the average, $F = ma$ for the ballast, but much more oscillation is evident in the acceleration indicating that the mass is not rigid. Figure 15, a typical plot of plate surface strain as a function of time, demonstrates that membrane action dominates bending in both dynamic and static plate deformation. The plate

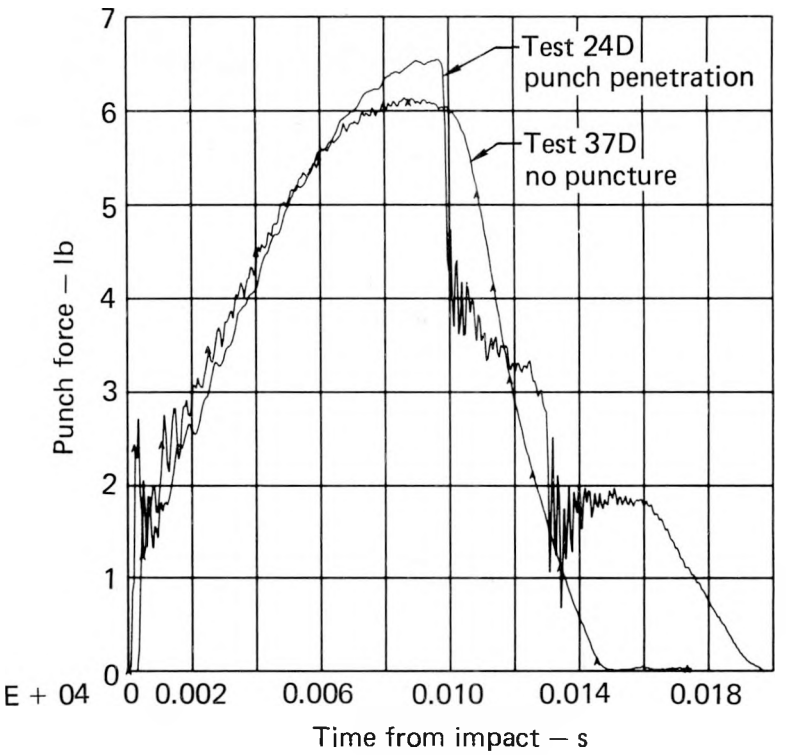

FIG. 13. Punch force vs time for 0.323-in. lead-backed plate with 0.938-in. punch.

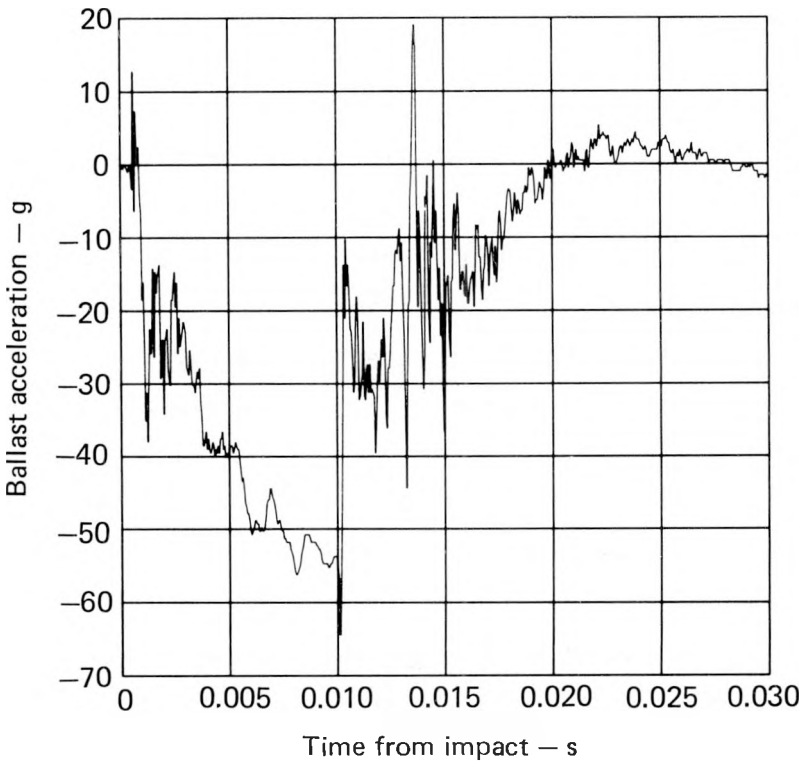

FIG. 14. Ballast acceleration vs time for 0.323-in. lead-backed SS plate and 0.938-in. punch.

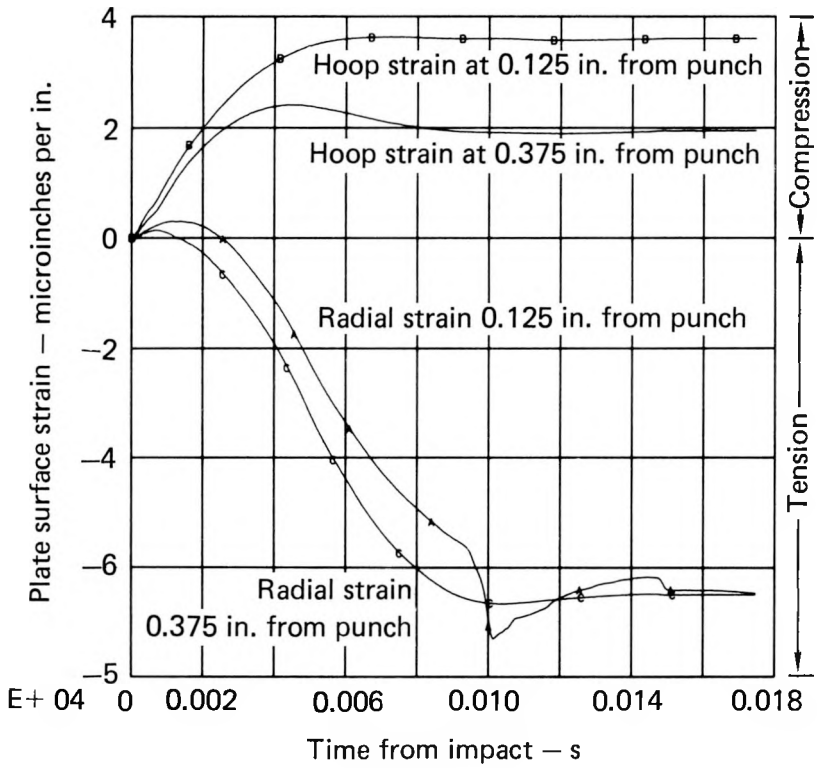

FIG. 15. Plate surface strains for 0.323-in. SS plate on 0.936-in. punch.

surface accelerometers did not provide consistent data. Large zero shifts make all plate surface acceleration data questionable.

In the static tests, the incipient puncture energy was determined by integrating the punch force vs deflection curves. In the dynamic tests, the incipient puncture energy was calculated in two ways. One way was to obtain the ballast velocity from its acceleration by integration and establish the decrease in kinetic energy at the instant of failure by calculating $1/2\ mv^2$. Subsequent integration of the velocity produced displacement. By eliminating the time parameter between the displacement vs time curve and the force vs time curve, we obtained a plot of force vs displacement. The second method of calculating incipient puncture energy involved integration of this force vs displacement curve. The drop height and weight provide an upper bound estimate of puncture energy. Figure 16 shows a plot of the acceleration from Fig. 14 integrated to produce ballast velocity. The initial condition for this integration is the impact velocity calculated from freefall conditions. The velocity time history exhibits much lower amplitude oscillation than does

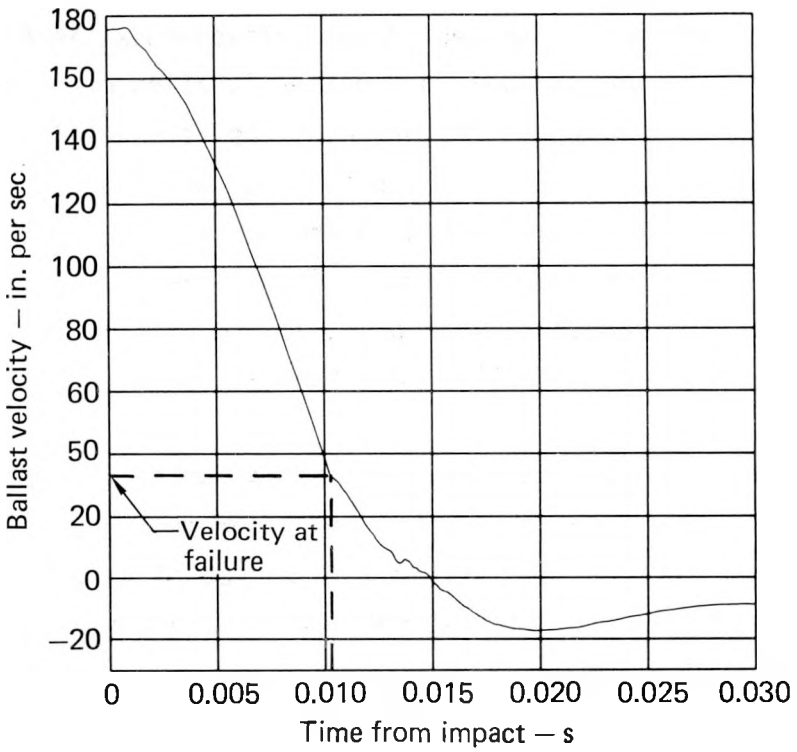

FIG. 16. Typical velocity time history for ballast.

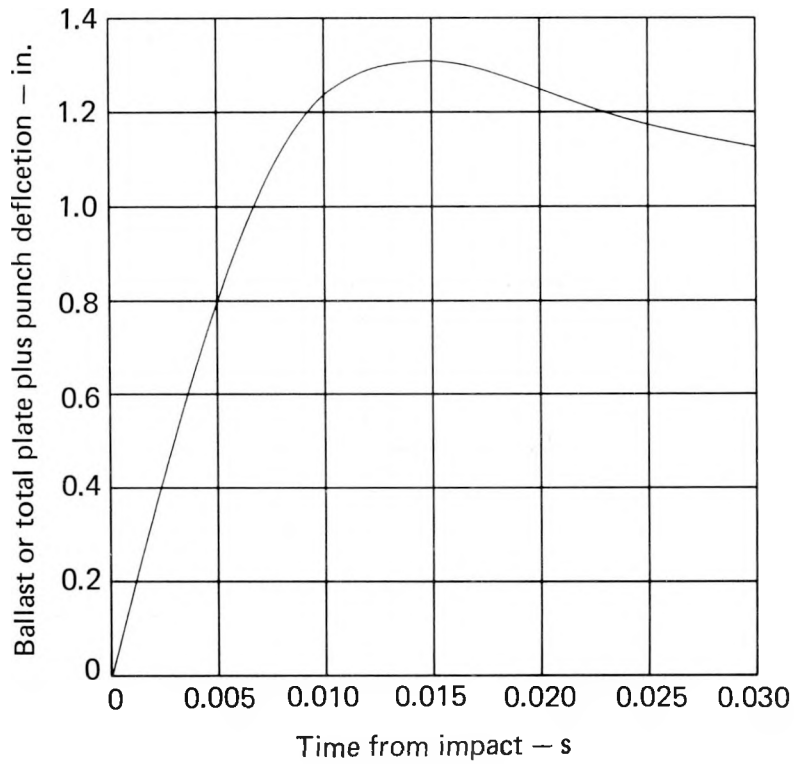

FIG. 17. Typical displacement time history of ballast.

the acceleration history. The second integration shown in Fig. 17 shows displacement vs time and is again a smoother function of time than the velocity. The elimination of time produces the force deflection curves of Fig. 18. Since deflection is a smooth function of time, the oscillations in the force-time history are reflected in the force-deflection curve. The integral of the force vs displacement of Fig. 18 is shown in Fig. 19. (Plots similar to Figs. 16 through 19 were produced for each dynamic test and are included with the raw data on the microfiche.)

Tables 2, 3, and 4 contain the test conditions for each test, a summary of the penetration conditions, and the penetration energies calculated by both methods. Table 2 includes the static lead-backed plates; Table 3 the uranium-backed and unbacked plates, both static and dynamic; and Table 4 all dynamic lead-backed plates.

The validity of the data is demonstrated by its consistency. Figure 20 shows how well the tests on 0.54-in.-thick lead-backed plates agree. Figure 21, in contrast, shows the largest degree of inconsistency observed in any series of

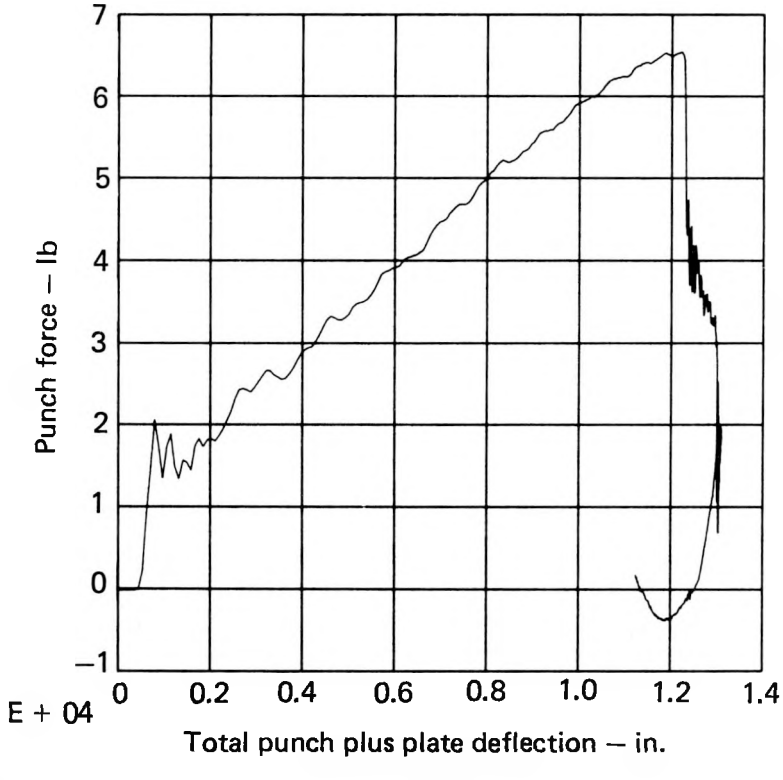

FIG. 18. Typical force vs deflection curve for dynamic test.

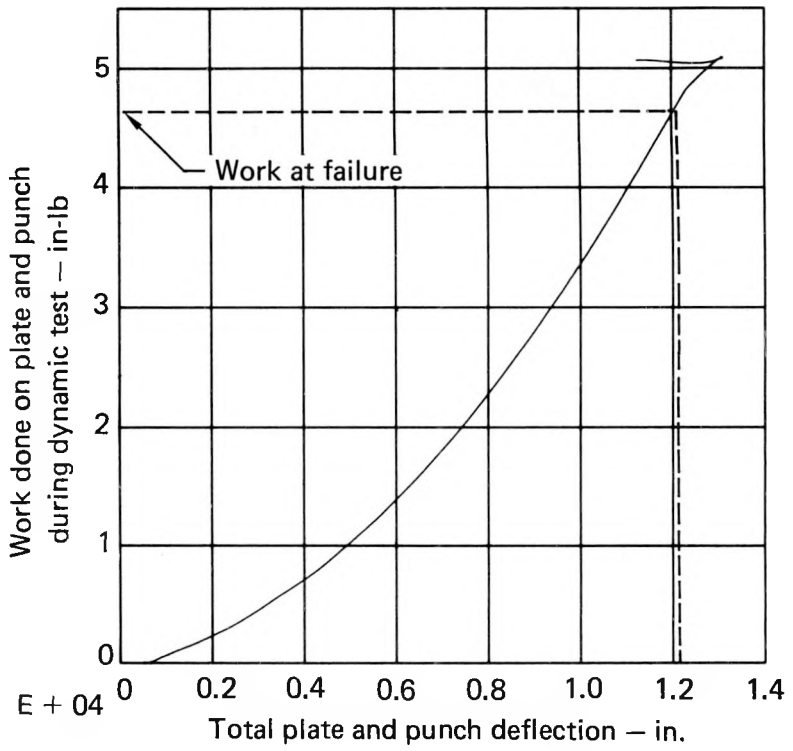

FIG. 19. Typical work calculated from force deflection plot.

TABLE 2. Static test conditions at penetration of lead-backed SS plates.

Plate thick., in.	Punch diam, in.	Test no.	Maximum Load, kips	Maximum defl., in.	Energy, 10^3 in.-lb	Remarks
0.05	0.6	1S	7.	0.61	2.3	
0.103	0.6	7S	13.8	0.80	5.6	
0.20	0.6	3S	25.5	1.11	15.3	
0.20	0.6	14S	25.3	1.03	13.8	
0.20	0.6	10ST	21.5	1.02	11.5	200°F
0.20	0.6	11ST	16.0	0.88	7.4	400°F
0.117	1.5	6S	39.0	1.01	23.3	
0.541	1.5	5S	175.	2.5	275.3	
0.535	1.5	13S	140.	1.56	129.2	Did not fail
0.540	1.5	20S	202.	2.35	307.2	Rounded punch
0.118	1.5	15S	40.0	1.12	26.0	Rounded punch
0.119	0.6	16S	15.5	0.78	6.85	0.936-in. backing
0.119	0.6	17S	16.7	0.65	7.18	1.5-in. backing

TABLE 3. Test conditions and results of uranium and unbacked SS plates.[a]

Plate thick., in.	Punch diam, in.	Test no.[b]	Drop wt, lb	Impact Vel., in./s	Impact Energy 10^3 in.-lb	Maximum Load, kips	Maximum defl., in.	Energy,[c] 10^3 in.-lb	Energy,[d] 10^3 in.-lb	Remarks
0.05	0.6	2S	-	-	-	31.0	0.39	8.5	-	
0.05	0.6	4S	-	-	-	34.0	0.52	11.5	-	
0.05	0.6	8S	-	-	-	29.5	0.78	14.0	-	Jointed
0.117	1.5	12S	-	-	-	200.	0.70	103.	-	
0.118	0.6	18S	-	-	-	12.5	0.97	5.28	-	Unbacked
0.05	0.6	8D	447	164.4	15.6	(39.5)	(0.54)	(14.8)	(15.2)	
0.05	0.6	11D	585	175.7	23.4	36.4	0.40	9.1	10.2	
0.05	0.6	9D	447	232.5	31.3	42.5	0.44	11.3	10.0	
0.05	0.6	17D	445	175.7	17.8	(30.7)	(0.84)	(18.6)	(18.0)	Jointed
0.05	0.6	40D	383	175.7	15.3	(33.5)	(0.78)	(18.6)	(15.6)	Jointed
0.05	0.6	38D	600	175.7	24.0	38.2	1.1	31.0	24.7	Jointed
0.117	1.5	30D	1938	215.2	116.	(194.)	(0.73)	(117.)	(118.)	
0.117	1.5	31D	1946	277.9	195.	217.	(0.66)	(110.)	(48.4)	
0.323	0.936	33D	1876	215.2	113.	(105.)	(1.7)	(138.)	(116.)	
0.323	0.936	32D	1894	277.8	189.	120.	1.89	174.	145.	
0.117	1.5	41D	602	175.7	24.1	31.1	1.34	21.6	16.6	Unbacked
0.117	1.5	39D	452	175.7	18.1	(29.9)	-	-	(18.5)	Unbacked

[a]Test results for plates that did not fail are calculated at the time of maximum punch force and are enclosed in parentheses.

[b]Test numbers with an S suffix denote static tests; those with a D suffix denote dynamic tests.

[c]Penetration energy is calculated as an integral of Fdx.

[d]Penetration energy is calculated as $m(V_o^2-V_f^2)/2+mg(\Delta x)$.

TABLE 4. Test conditions and results of dynamic tests on lead-backed SS plates.[a]

Plate thick, in.	Punch diam, in.	Test no.	Drop wt, lb	Impact Vel., in./s	Impact Energy, 10^3 in.-lb	Maximum Load, kips	Maximum defl., in.	Energy[b], 10^3 in.-lb	Energy[c] 10^3 in.-lb	Remarks
0.05	0.6	3D	445	60.6	2.11	(7.1)	(0.53)	(2.05)	(2.33)	
0.05	0.6	4D	445	63.7	2.34	(7.5)	(0.56)	(2.26)	(2.59)	
0.05	0.6	7D	445	68.1	2.67	no data				
0.05	0.6	10D	445	73.5	3.13	8.5	0.58	2.50	2.78	
0.05	0.6	2D	445	78.6	3.56	7.7	0.53	2.18	2.44	
0.05	0.6	1D	445	83.4	4.01	no data				
0.105	0.6	25D	448	87.9	4.48	no data				Did not fail
0.105	0.6	22D	685	87.9	6.85	no data				
0.2	0.6	21D	1000	87.9	(10.0)	(23.5)	(0.82)	(11.1)	(10.6)	
0.2	0.6	20D	1440	87.9	14.4	25.1	0.88	12.4	12.7	
0.2	0.6	19D	360	175.7	14.4	26.3	0.89	12.6	12.8	
0.2	0.6	6D	566	152.2	17.0	23.7	0.82	10.4	10.8	
0.2	0.6	5D	566	175.7	22.6	28.4	0.90	14.8	14.7	
0.415	0.6	16D	1200	175.7	48.0	(55.5)	(1.33)	(47.3)	(49.2)	
0.415	0.6	18D	1500	175.7	60.0	(65.0)	(1.57)	(62.2)	(61.1)	
0.415	0.6	27D	1815	175.7	72.6	(82.3)	(1.77)	(87.9)	(75.8)	
0.323	0.936	24D	1200	175.7	48.0	65.0	1.23	48.0	46.4	
0.323	0.936	23D	1500	175.7	60.0	68.9	1.38	57.6	55.1	
0.323	0.936	37D	1003	175.7	40.1	(61.4)	(1.24)	(51.0)	(41.4)	
0.117	1.5	14D	620	175.7	24.8	no data				Did not fail
0.117	1.5	12D	758	175.7	30.3	47.2	0.81	22.1	18.5	
0.117	1.5	13D	756	175.7	30.2	45.7	0.86	23.7	19.0	
0.260	1.5	26D	1815	175.7	72.6	86.8	1.28	68.4	60.3	
0.260	1.5	34D	1550	175.7	62.0	(85.0)	(1.39)	(74.8)	(64.1)	
0.260	1.5	35D	1573	175.7	62.9	81.5	1.12	64.0	51.8	200°F
0.260	1.5	36D	1201	175.7	48.0	67.0	1.31	56.7	45.3	400°F
0.540	1.5	28D	1831	301.8	216.	(175.)	(2.1)	(247.)	(220.)	
0.540	1.5	29D	1957	301.8	231.	177.	2.06	243.	230.	

[a]Test results for plates that did not fail are calculated at the time of maximum punch force and are enclosed in parentheses.

[b]Penetration energy is calculated as an integral of Fdx.

[c]Penetration energy is calculated as $m(V_o^2-V_f^2)/2+mg(\Delta x)$.

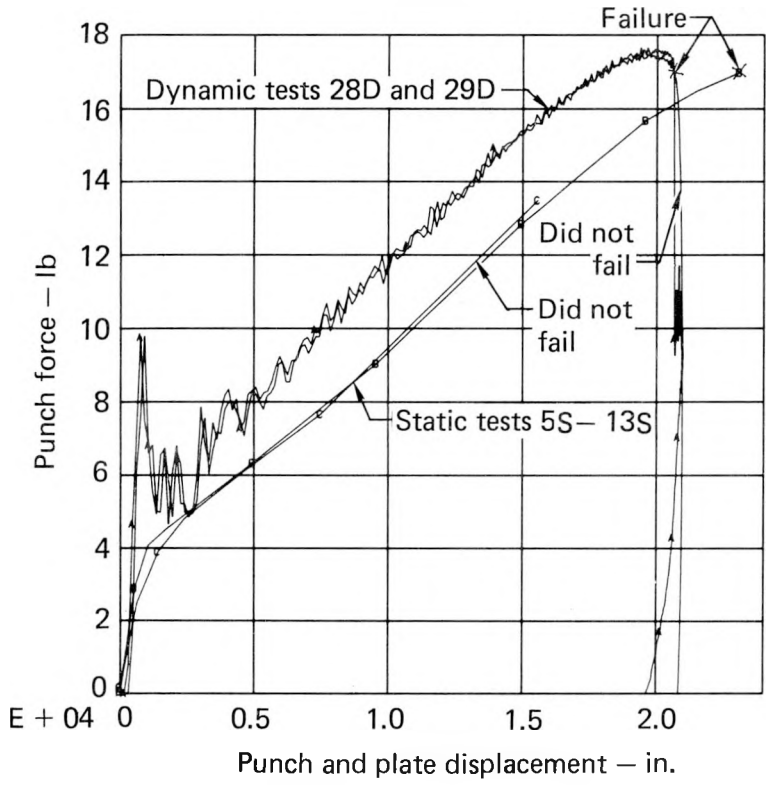

FIG. 20. Example of data consistency for tests on 0.54-in. lead-backed SS plates.

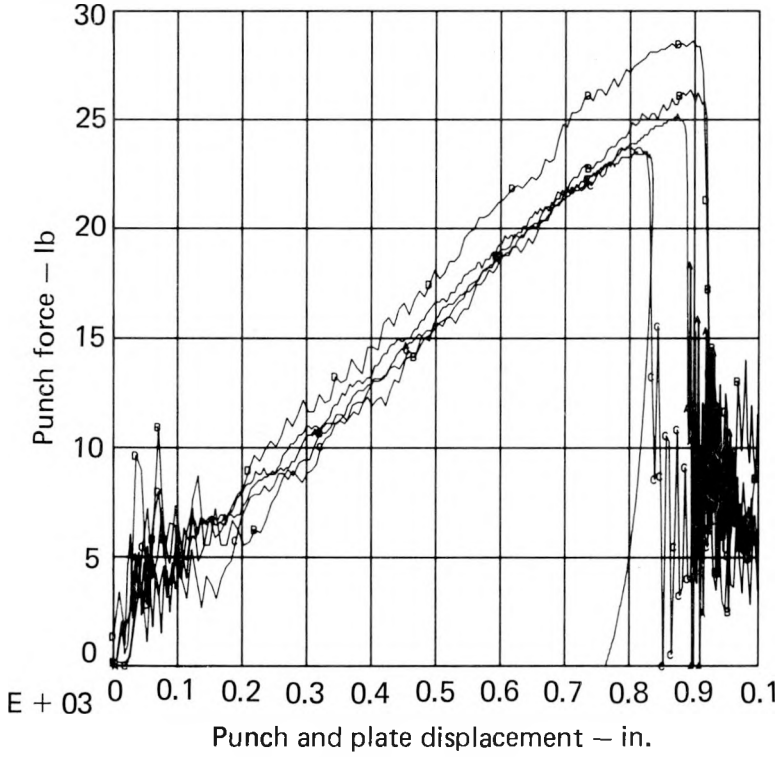

FIG. 21. Example of largest inconsistency in dynamic tests of 0.2-in. SS plates (Tests 5D, 6D, 19D, 20D, 21D).

dynamic tests. Not enough static tests were conducted with identical parameters to establish reliable statistics, but the dynamic tests of lead-backed plates show very good repeatability. Inconsistencies in the uranium material produced larger variations in test results than in the lead-backed plates.

All of the backed plates tested during this project have exhibited force deflection curves that can be approximated by two straight lines. Figures 22 and 23 show the static force deflection curves for lead-backed plates penetrated using two sizes of punches. Figure 24 shows similar curves for the static puncture of urnamium-backed plates. The dynamic force deflection curves for backed plates also show this bilinear characteristic. The point of slope change in this curve seems to be determined by the backing material and thickness. Static and dynamic tests of unbacked plates produce force deflection curves like those shown in Fig. 25, which do not exhibit the bilinear behavior of backed plates. The unbacked plates appear to have very little plate bending behavior; their behavior is mostly membrane response.

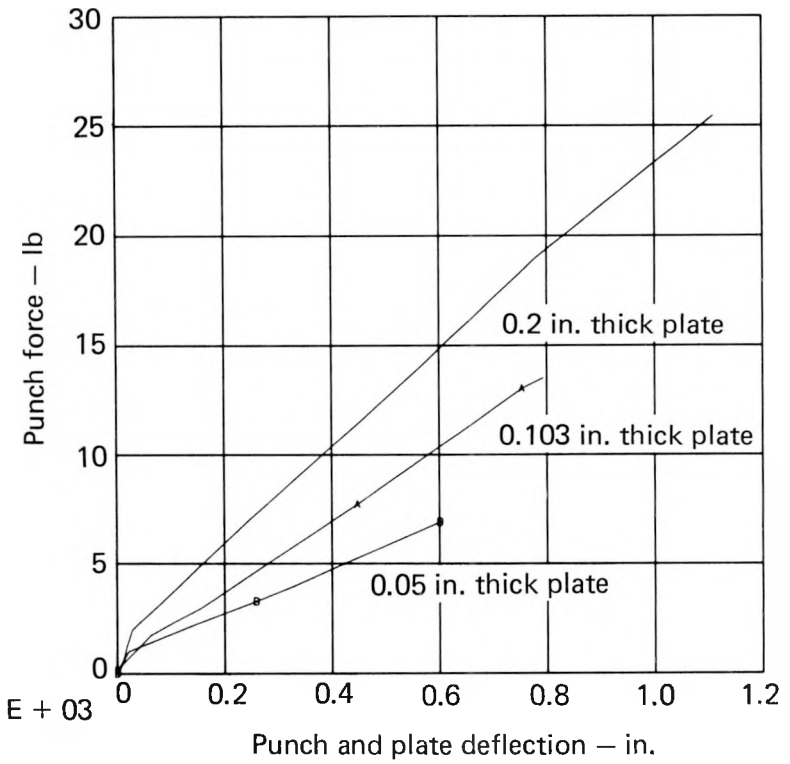

FIG. 22. Typical static response of lead-backed SS plates with 0.6-in. punch.

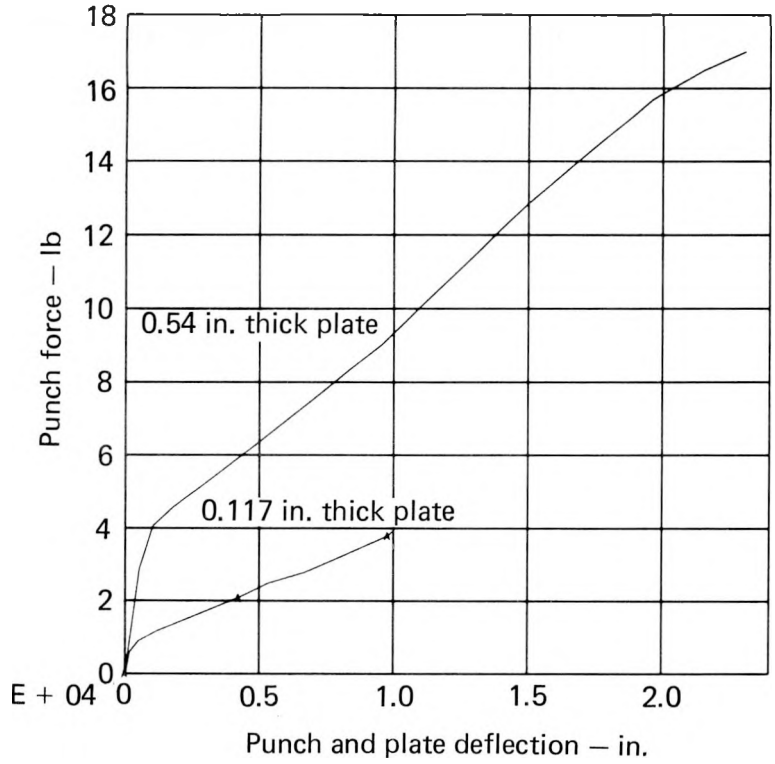

FIG. 23. Typical static response of lead-backed SS plates with 1.5-in. punch.

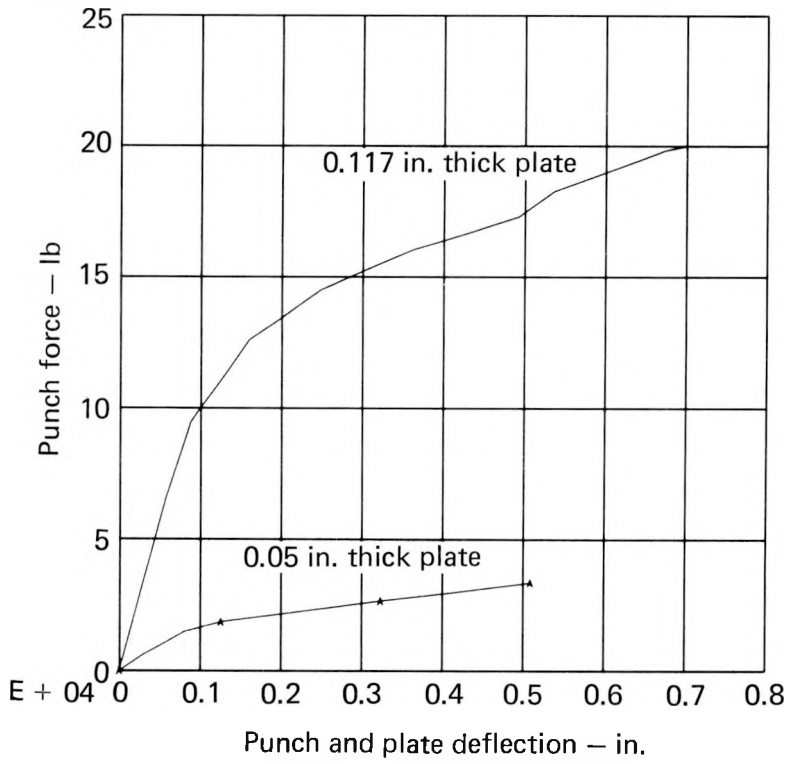

FIG. 24. Typical response of uranium-backed SS plates.

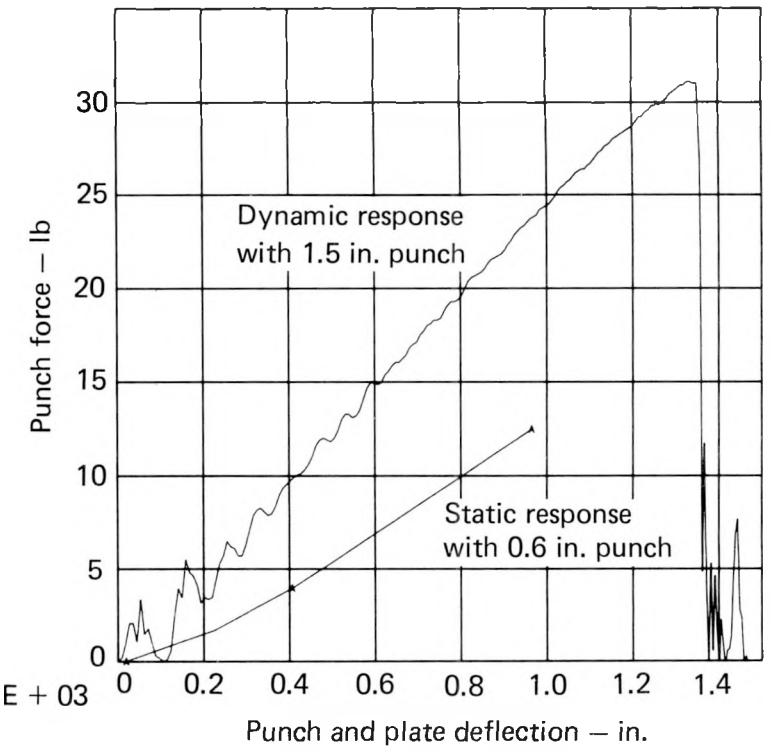

FIG. 25. Typical static and dynamic response of 0.117-in. unbacked SS plates.

Some of the most interesting data comparisons are those of static and dynamic tests of identical plates. Definite variations between the static and dynamic force deflection curves are observed for all configurations. A typical static and dynamic curve for each configuration for which static and dynamic tests were conducted is shown in Figs. 20 and 26 for lead-backed plates and in Fig. 27 for uranium-backed plates. We have not drawn any conclusions about the differences between the static and dynamic force deflection curves. The force deflection curves from two tests at the same impact energy, but with impact velocities varying by a factor of two, show no strain rate effects. Figures 28 and 29 show results from tests at two different impact velocities on 0.2-in. lead-backed plates in which the mass of one is exactly four times the mass of the second. The force-time histories shown in Fig. 28 demonstrate the shift in the fundamental natural frequency and the associated strain rate change. Figure 29 demonstrates the close agreement between the force deflection curves for these two tests and shows that dynamic puncture force and energy are insensitive to drop height within the range of our tests.

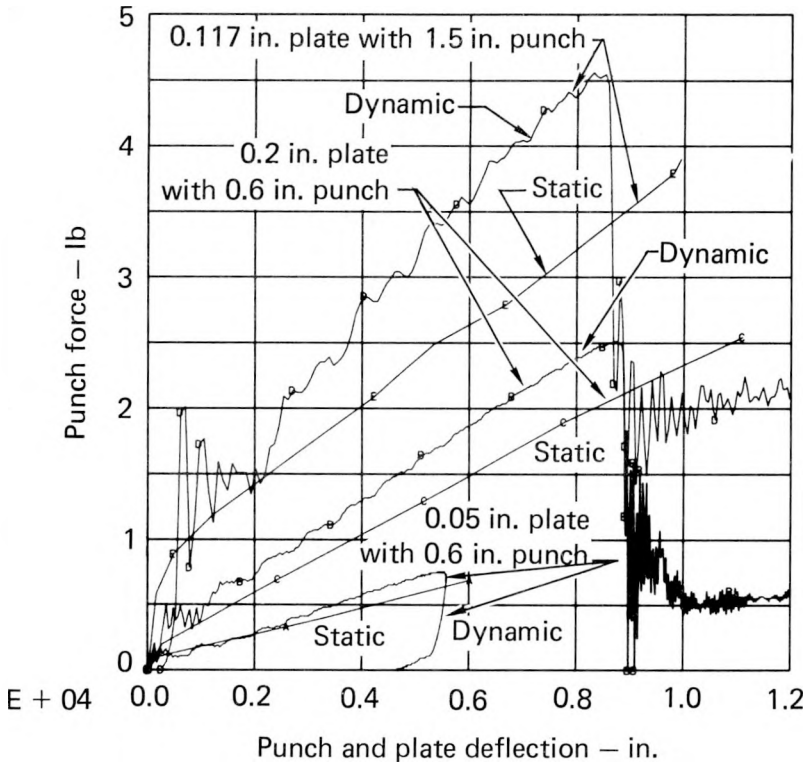

FIG. 26. Comparisons between static and dynamic response of lead-backed SS plates.

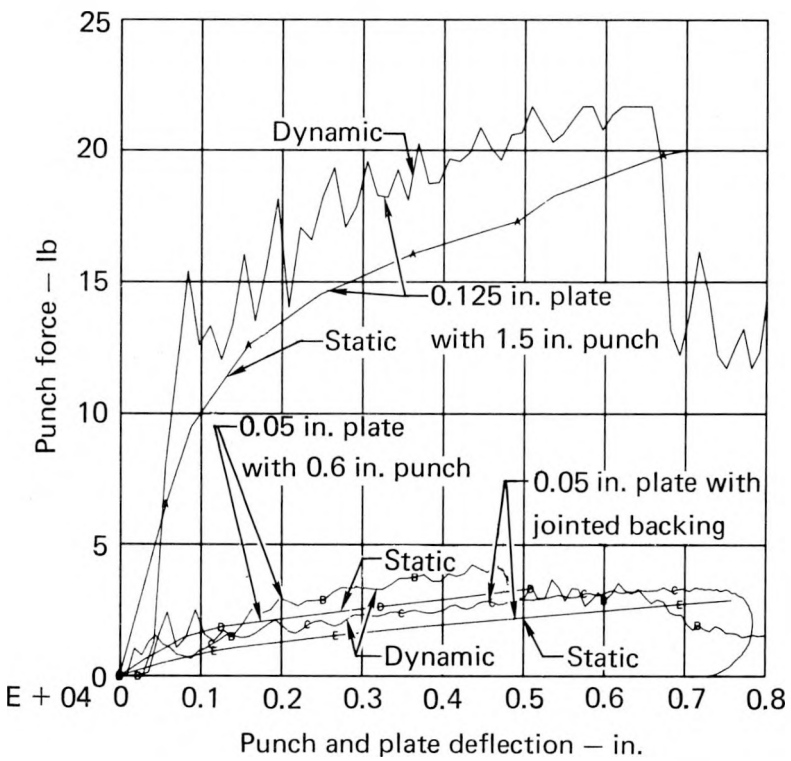

FIG. 27. Typical static and dynamic comparisons for uranium-backed SS plates.

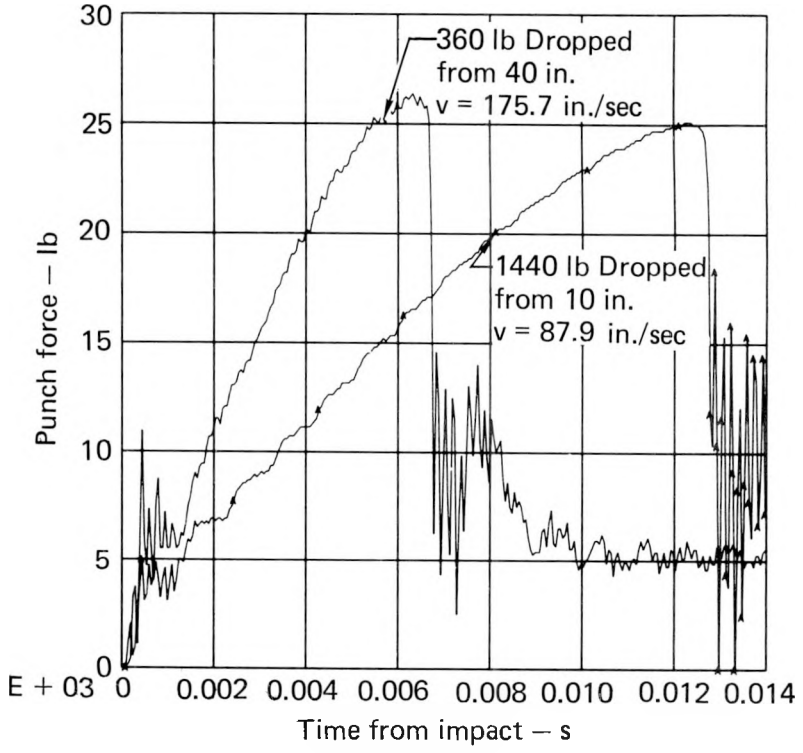

FIG. 28. Punch force vs time for two 0.2-in. SS plates dropped at same energy (14,400 in.-lb).

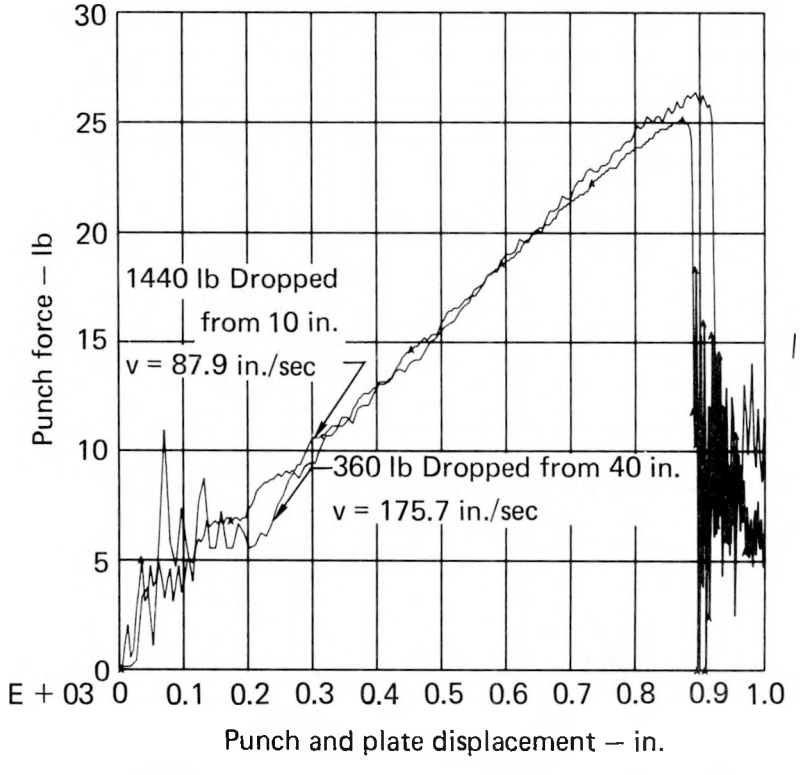

FIG. 29. Punch force vs deflection for two 0.2-in. SS plates at different velocity.

The effect of test temperature on the force vs deflection curves for static and dynamic tests is shown in Figs. 30 and 31. In the static tests, both deflection and the force at failure decrease with increasing test temperature. In the dynamic tests with a larger punch and thicker backing, the failure force also decreases with temperature. The deflection at failure at 200°F is lower than at room temperature, but the deflection at 400°F is higher than at room temperature. In addition, at 200°F the force at any deflection is higher than the force at room temperature and the same deflection. This apparently anomalous result has not been explained except that the accelerations and load cell readings do not seem to agree as well on the 200°F test as they do on the other tests.

For one geometry only, in the static tests, the backing thickness was varied from 2.5 times the punch diameter to zero. Comparative force deflection curves for these tests are shown in Fig. 32. The effect of rounding the punch edge is shown in Figs. 33 and 34. Although the square punch edge deforms considerably for the thicker plates, there seems to be some increase in the puncture force and energy as a result of using a rounded edge punch. No

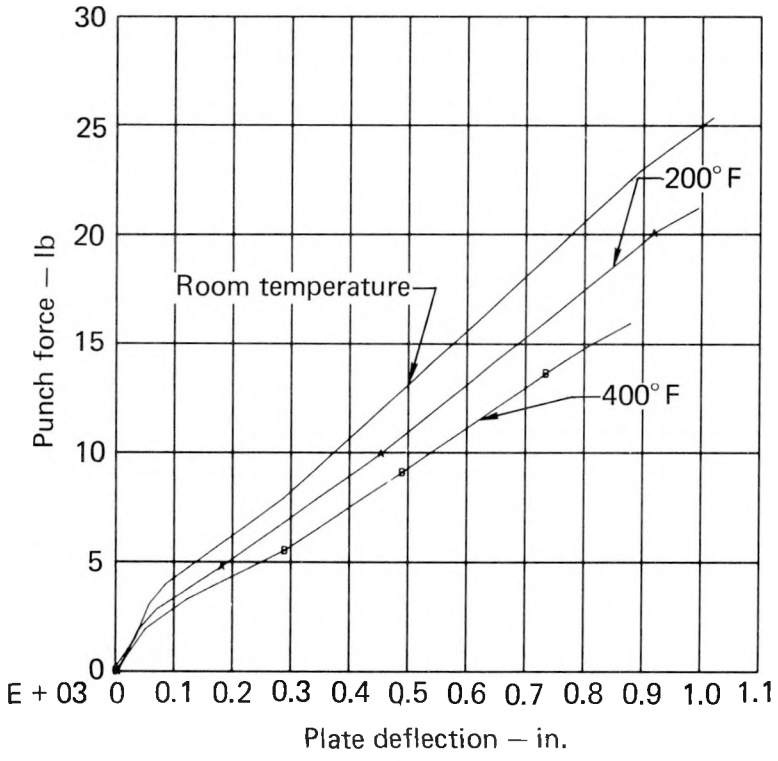

FIG. 30. Effects of temperature on static puncture of 0.2-in. lead-backed SS plates and 0.6-in. punch.

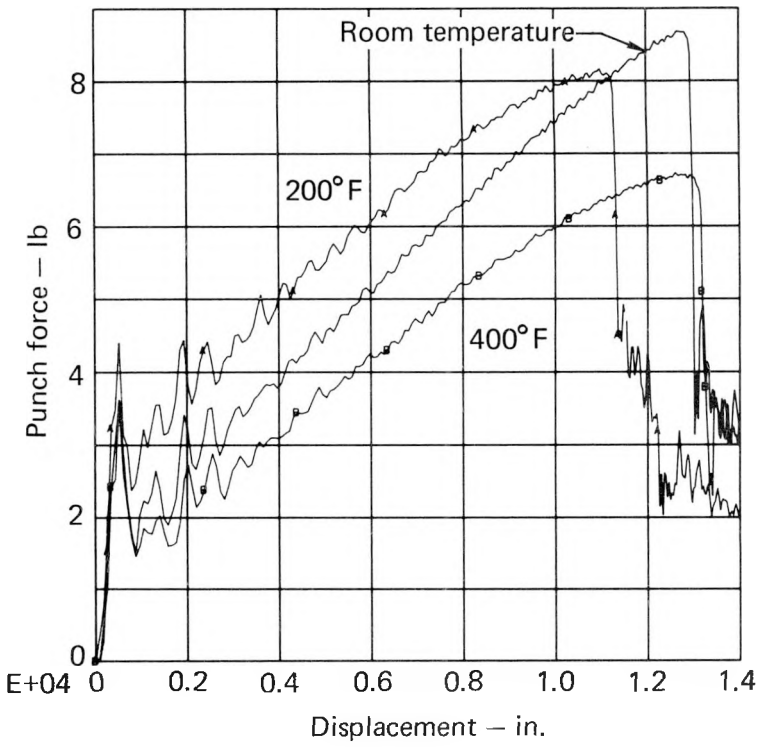

FIG. 31. Effects of temperature on dynamic puncture of 0.260-in. lead-backed SS plate with 1.5-in. punch.

significant increase was observed in the thin plate. The federal regulations allow the 6-in.-diam punch a 1/4-in. edge radius. Scaling this by 1/4 results in a 1/16-in. edge radius on the 1.5-in.-diam punch. Holding the edge radius tolerance for smaller scale punches was not attempted, and all of the remaining punches used were specified to have a sharp edge.

Since uranium is a viable alternative to lead for gamma shielding in modern shipping containers, comparison of the relative puncture resistance is valuable. These tests have shown that while our uranium-backed plates are not inpenetrable by mild steel punches, they are significantly less penetrable than the lead-backed plates. The use of uranium backing significantly increase the stiffness of the test specimens. Figure 35 shows the punch force-time histories of two 0.05-in.-thick plates dropped on 0.6-in.-diam punches. The uranium-backed plate has a much shorter natural period of vibration than the lead-backed plate. The uranium-backed plates in these tests failed at 1.8 to 4.9 times the punch force required to fail the

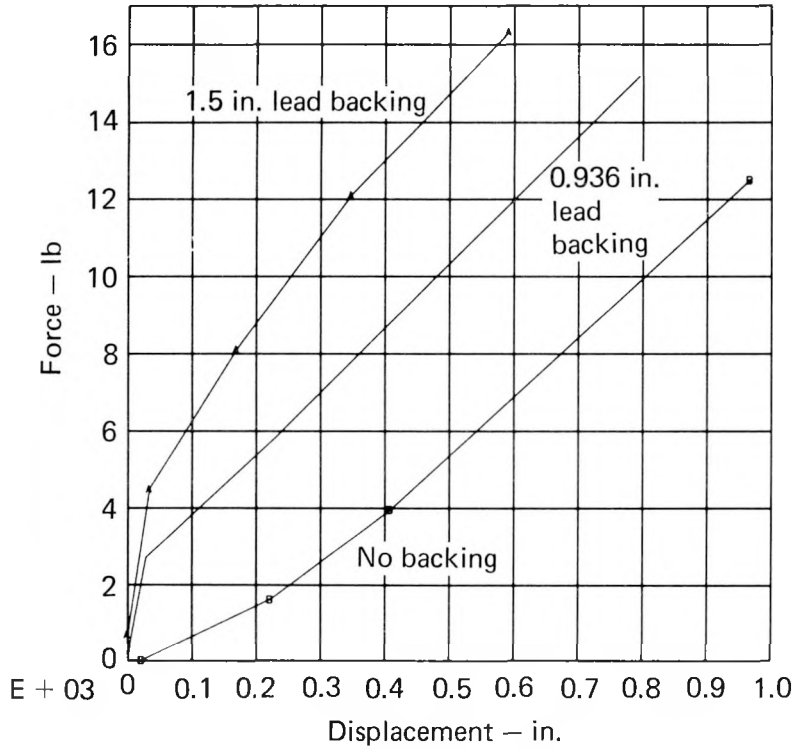

FIG. 32. Static test data: effect of backing on 0.119-in. SS plate with 0.6-in. punch.

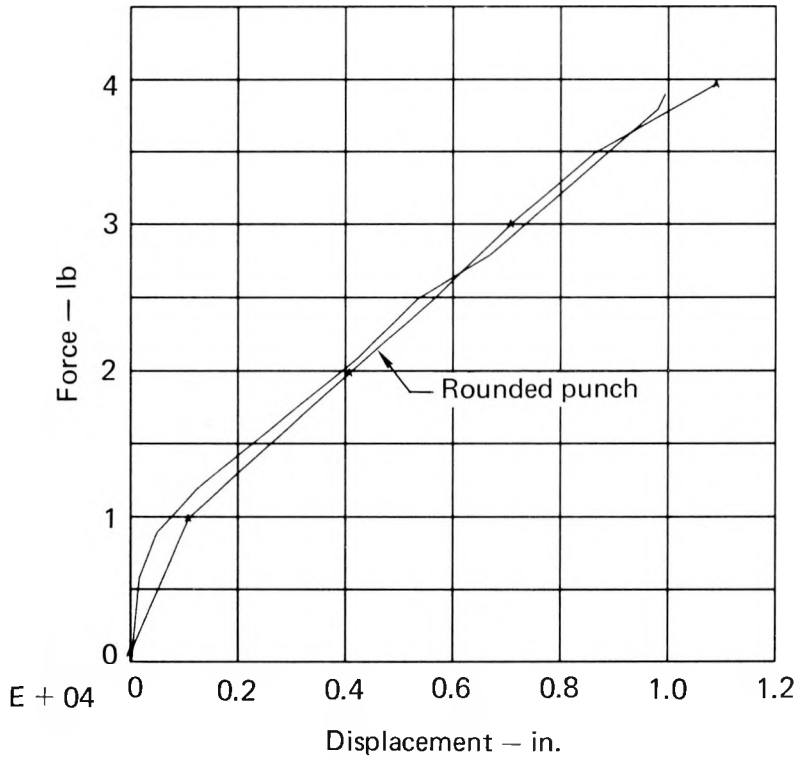

FIG. 33. Static test data: effect of rounded punch on lead-backed 0.117-in. SS plate with 1.5-in. punch.

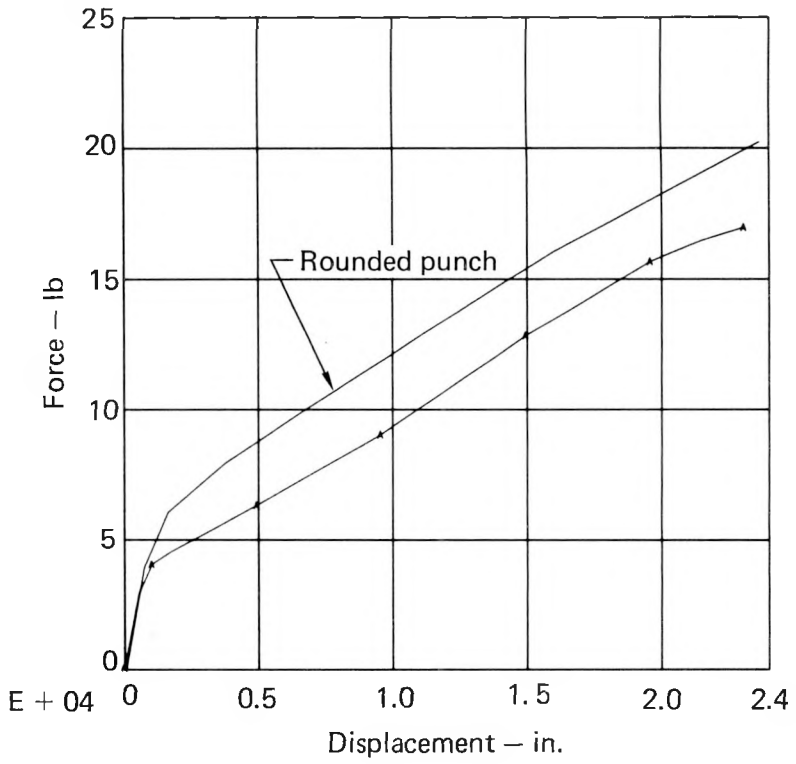

FIG. 34. Static test data: effect of rounded punch on 0.540-in. SS plate with 1.5-in. punch.

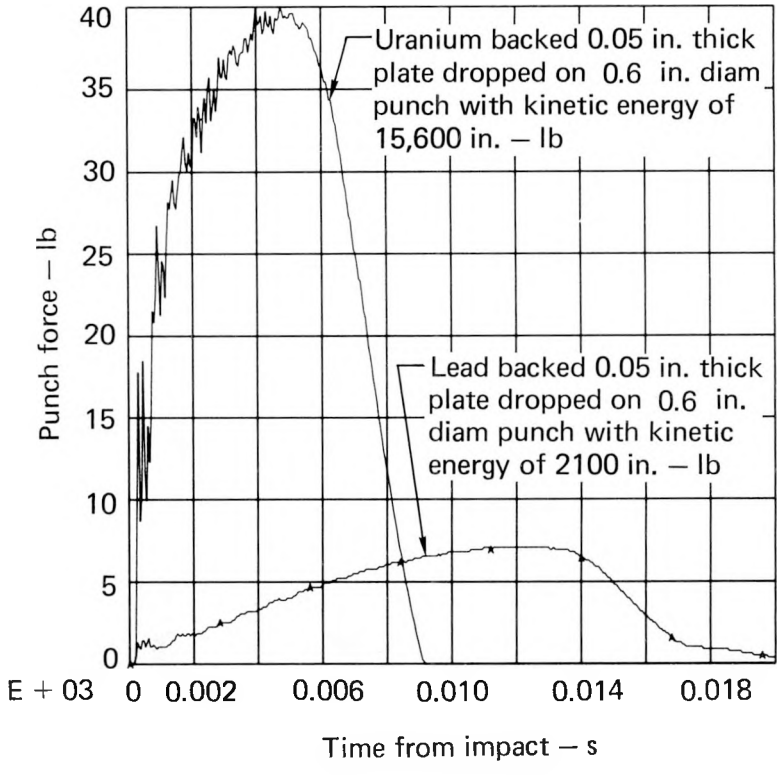

FIG. 35. Comparison between lead- and uranium-backed plates.

equivalent lead-backed plates. Although the uranium-backed plates absorbed between 3.3 and 4.8 times more energy than equivalent lead-backed plates, it is important not to generalize to other configurations without careful analysis.

Figure 36 shows the punch force vs plate deflection plots for all of the 0.05-in. uranium-backed plates tested. In comparison, Fig. 37 shows the punch force vs plate deflection for the tests in which the punch diameter to plate thickness was the same as the plates of Fig. 35 except that the punch diameter was 1.5 in. instead of 0.6 in. The effect of jointed backing is shown in Fig. 38 for static tests of uranium-backed plates. Figure 39 shows similar comparisons for dynamic tests of jointed and unjointed uranium-backed plates. Figure 40 shows the force deflection curves for the dynamic puncture of thicker uranium-backed plates.

Besides being more resistant than lead-backed plates to penetration, uranium-backed plates differ in their mode of failure. In lead-backed plates, the mode of failure is an annular shear fracture in the test plate near the circumference of the punch. The "coin" that this failure produces is then pushed into the adjacent surface of the lead backing until the load is reduced. In no case does the fracture propagate to the rear surface of the lead. In the case of uranium-backed plates, the backing appears to fracture first, followed by failure of the test plate. Figure 41 shows the tensile fracture of the back side of a uranium plate. Figure 42 shows front face damage to three uranium plates.

Although the yield strength of the punches is slightly greater than that of the plates, punch yielding occurred on all tests. As the punch diameter to plate thickness ratio, d/t, decreases, punch deformation increases in relation to the punch's ability to penetrate the plate. In the series of dynamic tests where the d/t ratio was 1.45, none of the plates failed. Figure 43 shows the conical contact area that forms near the edge of a 0.6-in. punch when successively greater impact energy is applied. (The plates also display a conical contact area.) Because of the softness of the mild steel punches, none of the plates that withstood puncture exhibited shear fracture on the punch side of the plate before fracture became evident on the rear face of the plate.

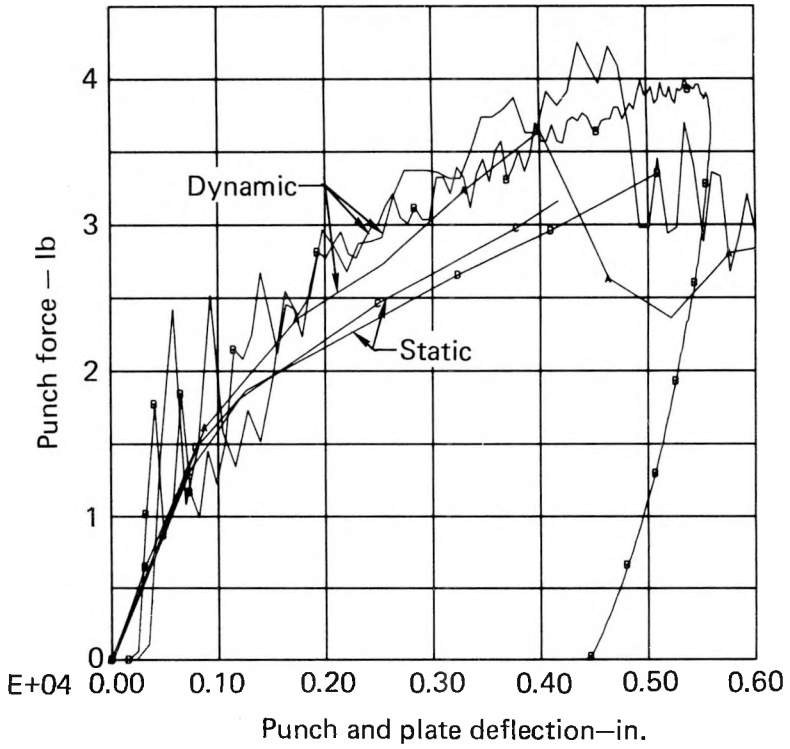

FIG. 36. Force vs deflection for all 0.05-in. uranium-backed SS plates.

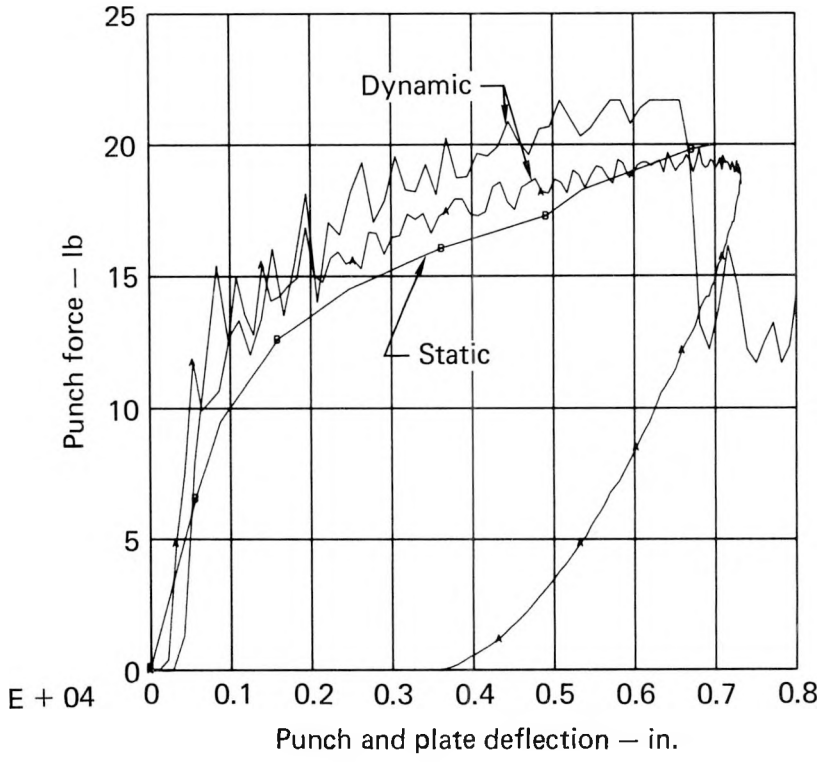

FIG. 37. Force vs deflection for all 0.117-in. uranium-backed SS plates.

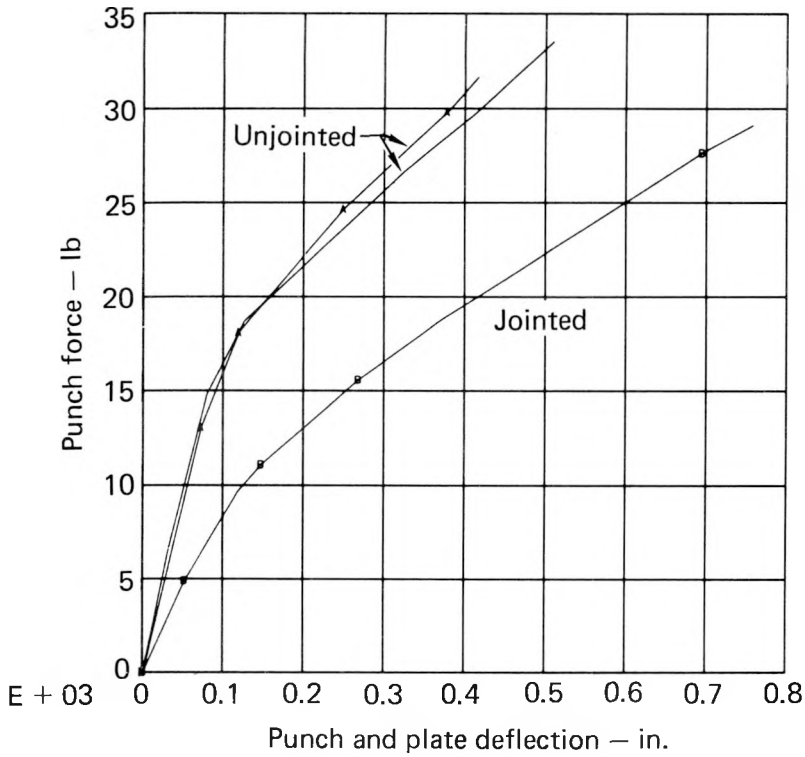

FIG. 38. Comparison between static tests of jointed and unjointed uranium backing.

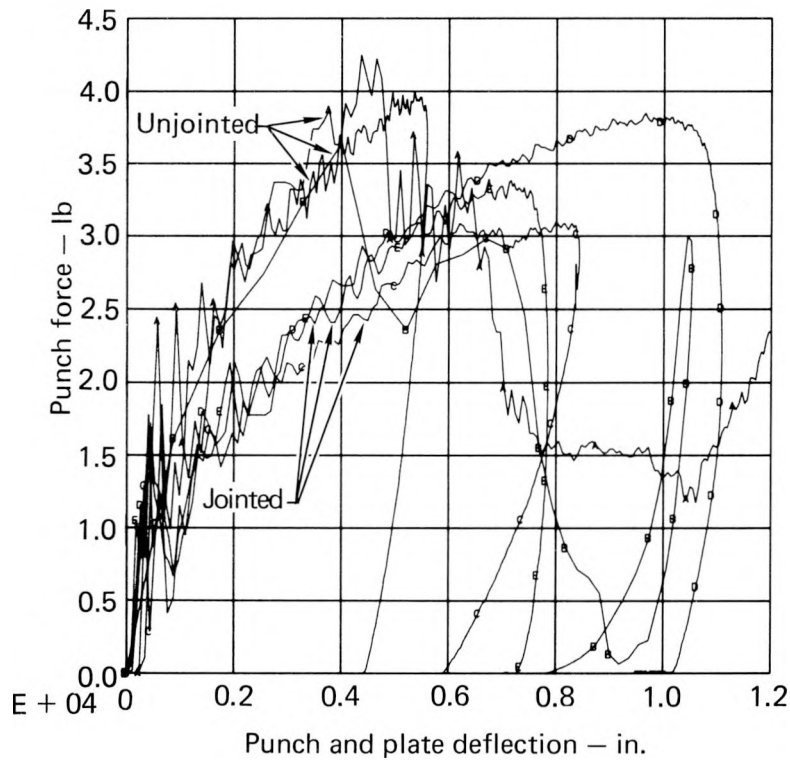

FIG. 39. Comparison between dynamic tests with jointed and unjointed uranium backing.

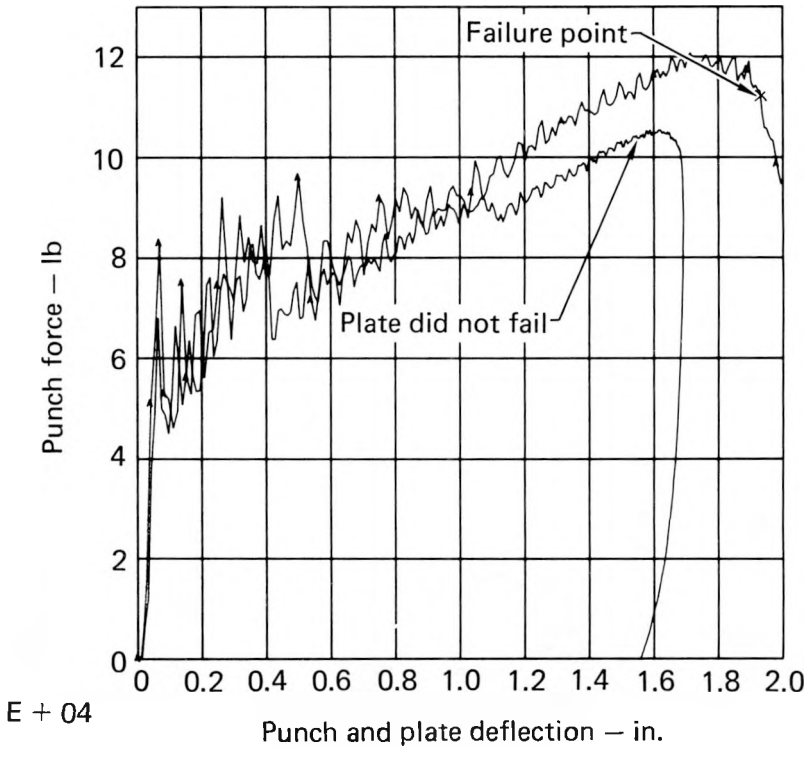

FIG. 40. Force vs deflection for thicker uranium-backed SS plates.

FIG. 41. Fractured uranium plate.

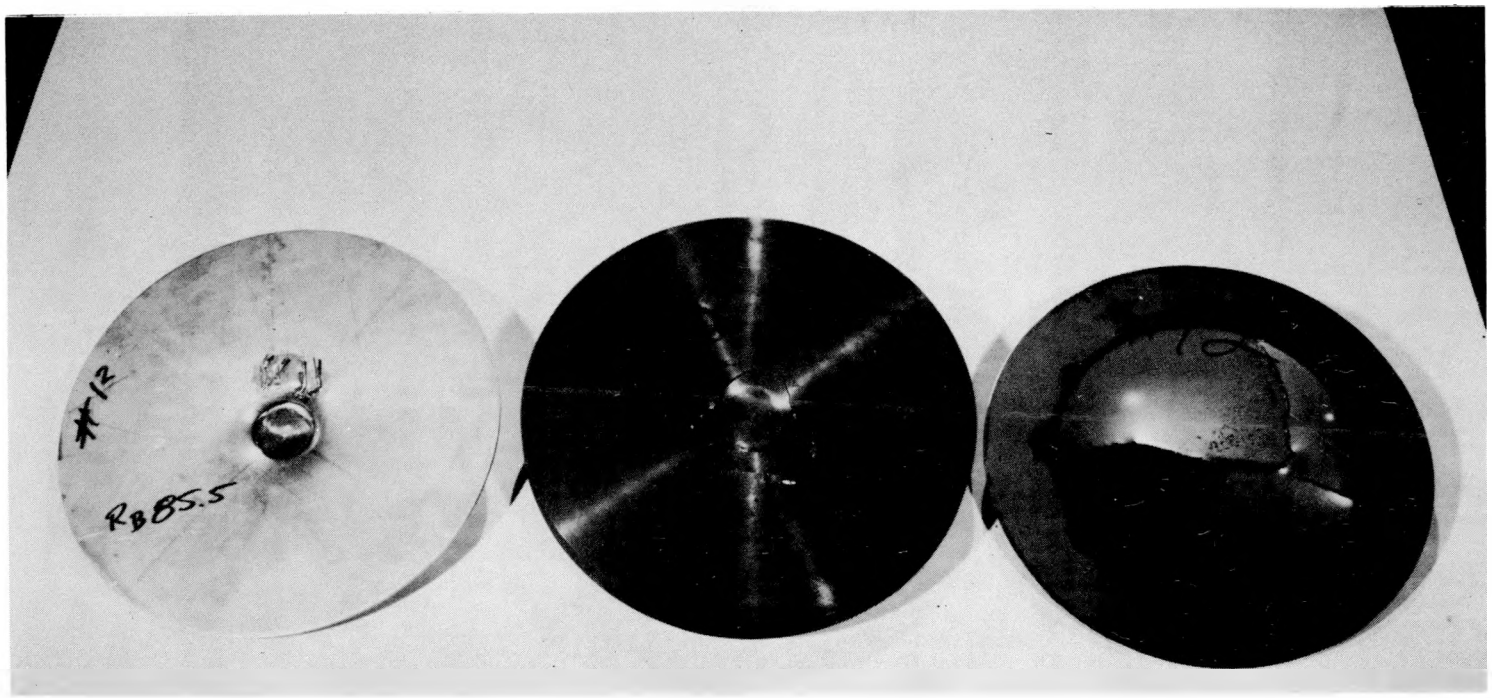

FIG. 42. Front face damage of uranium plate.

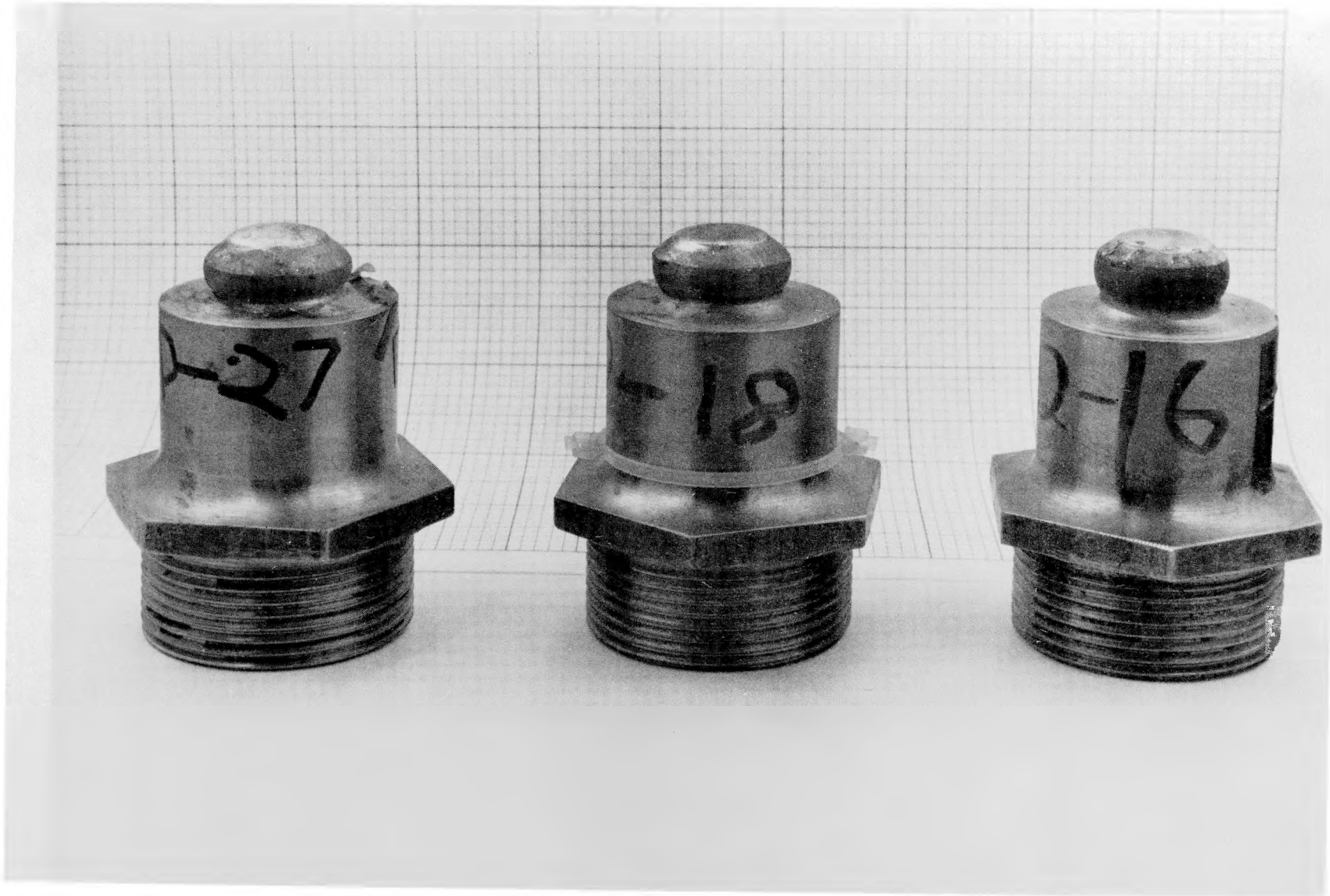

FIG. 43. Severely deformed punches.